JOURNAL OF PETROLOGY | VOLUME 53 | NUMBER 11 | PAGES 2381–2409 | 2012 | doi:10.1093/petrology/egs047

Petrogenesis of Tertiary Alkaline Magmas in the Siebengebirge, Germany

S. JUNG[1]*, K. VIETEN[2], R. L. ROMER[3], K. MEZGER[4], S. HOERNES[2] AND M. SATIR[5]

[1]DEPARTMENT GEOWISSENSCHAFTEN, MINERALOGISCH-PETROGRAPHISCHES INSTITUT, UNIVERSITÄT HAMBURG, 20146 HAMBURG, GERMANY

[2]MINERALOGISCH-PETROLOGISCHES INSTITUT DER UNIVERSITÄT BONN, POPPELSDORFER SCHLOß, 53115 BONN, GERMANY

[3]GEOFORSCHUNGSZENTRUM POTSDAM, TELEGRAFENBERG, B 126, D-14473 POTSDAM, GERMANY

[4]INSTITUT FÜR GEOLOGIE, UNIVERSITÄT BERN, BALTZERSTRASSE 1+3, CH-3012 BERN, SWITZERLAND

[5]INSTITUT FÜR GEOWISSENSCHAFTEN, UNIVERSITÄT TÜBINGEN, SIGWARTSTR. 10, 72076 TÜBINGEN, GERMANY

RECEIVED JULY 8, 2011; ACCEPTED JUNE 13, 2012
ADVANCE ACCESS PUBLICATION SEPTEMBER 12, 2012

Basanites from the Tertiary Siebengebirge area of Germany (part of the Central European Volcanic Province; CEVP) have high Mg# (>0·60), moderate to high Cr (>300 ppm) and Ni (>200 ppm) contents and strong light rare earth element enrichment, but systematic depletion in Rb and K relative to trace elements of similar compatibility in anhydrous mantle. Rare earth element melting models can explain the petrogenesis of these basanites in terms of partial melting of a spinel peridotite source containing residual amphibole. It is inferred that amphibole, indicated by the relative K and Rb depletion and the melting model, was precipitated in the spinel peridotite lithospheric mantle beneath the Siebengebirge, by metasomatic fluids or melts from a rising mantle diapir or plume. Alkali basalts and more differentiated rocks have lower Mg# and lower abundances of Ni and Cr, and have undergone fractionation of mainly olivine, clinopyroxene, Fe–Ti oxides, amphibole and plagioclase. Most of the basanites and alkali basalts approach the Sr–Nd–Pb isotope compositions inferred for the European Asthenospheric Reservoir component. Trace element constraints (i.e. low Nb/U and Ce/Pb ratios) and the Sr–Nd–Pb isotope composition of the differentiated rocks indicate that assimilation of lower crustal material has modified the composition of the primary mantle-derived magmas. High $^{207}Pb/^{204}Pb$ ratios in the differentiated lavas point to assimilation of ancient lower crustal components having high U/Pb and Th/Pb ratios. Relatively shallow melting of inferred amphibole-bearing spinel peridotite sources may suggest an origin from the metasomatized part of the thermal boundary layer. Application of new thermobarometric equations for the basaltic magmas indicates relatively normal mantle potential temperatures (1300–1400°C); thus the inferred mantle 'baby plume' or 'hot finger' is not thermally anomalous.

KEY WORDS: *alkali basalts; continental volcanism; crustal contamination; partial melting; Siebengebirge*

INTRODUCTION

Despite decades of intense investigation, significant questions remain on the origin and evolution of rift-related alkaline basalts. In such areas, the volcanic products represent relatively small volumes of juvenile crust emplaced over short time periods, but the nature of the source and the processes that form these magmas are not well understood. Although many of these usually sodium-dominated basalts have a chemistry similar to many ocean island basalts (OIB) (Allègre *et al.*, 1981; Fitton & Dunlop, 1985; Thompson & Morrison, 1988, among many others), it is still highly debated whether the primary source of the

*Corresponding author: Phone: +49(0)40-42838-2061. Fax: +49(0)40-42838-2422. E-mail: stefan.jung@mineralogie.uni-hamburg.de

melt is the shallow enriched subcontinental lithospheric mantle (SCLM), the shallow asthenospheric mantle or deep plume-related mantle. The similarity to many OIB magmas has led to the proposal that the convecting asthenosphere is the source of most sodic alkaline magmas, in which the isotope compositions and the trace element enrichment reflect mixing of enriched lithospheric mantle and crustal material into the asthenosphere by delamination and subduction (White & Hofmann, 1982; McKenzie & O'Nions, 1983; Hart, 1988). Also important is whether the variations in the chemical and isotopic compositions of the magmas are the result of mixing of different mantle endmembers or the result of crustal contamination. To understand and model the formation and evolution of rift-related volcanic provinces, we need to be able to discriminate between the various potential mantle sources of the basalts and the sources of contamination.

Much of the controversy on the origin of rift-related provinces revolves around the interpretation of the trace element characteristics and Sr, Nd and Pb isotopic composition of the basalts. This information has yielded partly ambiguous results because both crust and enriched mantle can impart similar characteristics and because the chemical and isotopic compositions of the various endmember mantle reservoirs are created, at least in part, through crustal recycling or are susceptible to modification through metasomatism. Hence, one interpretation is that the lithospheric signatures of continental basalts are primarily signs of contamination of sublithospheric melts by either lithospheric mantle or continental crust. Another interpretation is that melting of continental lithosphere is aided by the presence of water and/or low-melting temperature mafic veins that will allow the lithospheric mantle to be the main contributor to continental basaltic volcanism (Gallagher & Hawkesworth, 1992; Harry & Leeman, 1995; Pilet *et al.*, 2008).

For the Central European Volcanic Province (CEVP), the volcanic products converge on a common source composition when plotted in conventional Sr–Nd–Pb isotope diagrams. This common source has been termed PREMA (PREvalent MAntle; Wörner *et al.*, 1986), the European Asthenospheric Reservoir (EAR, Cebriá & Wilson, 1995), Low Velocity Component (LVC; Hoernle *et al.*, 1995) or CMR (Common Mantle Reservoir; Lustrino & Wilson, 2007) and is believed to represent a plume-related reservoir. Other, probably minor, reservoirs are believed to originate in the SCLM (Cebriá & Wilson, 1995; Granet *et al.*, 1995; Hoernle *et al.*, 1995). Support for a deep mantle origin for the most primitive magmas comes from high-resolution mantle seismic tomography showing low-velocity domains in the mantle at various depths. Consequently, an asthenospheric origin for the European volcanism linked to a series of diapiric mantle upwellings has been suggested (Granet *et al.*, 1995; Hoernle *et al.*, 1995; Goes *et al.*, 1999; Ritter *et al.*, 2001; Wilson & Patterson, 2001; Keyser *et al.*, 2002). For the Rhenish Massif, a columnar low P-wave velocity anomaly has been detected beneath the Eifel (Ritter *et al.*, 2001). This 100 km wide structure extends down to 400 km depth and could be interpreted to be equivalent to an excess mantle temperature of 150–200°C in the absence of volatiles or partial melt. It should be noted that such geophysical considerations require that the upper mantle is isochemical and isomineralogical, which is certainly an oversimplification. In addition, the seismic wave anomalies are discontinous beneath the Eifel and are more influenced by chemical and mineralogical anomalies rather than representing temperature gradients. Hence, the reported excess temperature should be viewed as an upper limit. On the other hand, based on xenolith studies, the metasomatized lithospheric mantle can be a potential source of the mafic lavas. Partial melting of such zones of metasomatized lithospheric mantle, combined with interaction between asthenospheric melts and lithospheric melts, has been proposed to explain the geochemical characteristics of the most primitive mafic alkaline rocks of the CEVP (Wilson & Downes, 1991; Wilson & Patterson, 2001). In addition, crustal contamination of the mantle-derived magmas has been widely documented within the CEVP (Massif Central: Wilson *et al.*, 1995a; Vogelsberg: Jung & Masberg, 1998; Bogaard & Wörner, 2003; Jung *et al.*, 2011; Rhön: Jung & Hoernes, 2000; Jung *et al.*, 2005; Urach–Hegau: Blusztajn & Hegner, 2002; Westerwald: Haase *et al.*, 2004).

Neither comprehensive whole-rock geochemical data nor sufficient Sr–Nd–Pb isotopic data have been published for the Tertiary Siebengebirge volcanic field. Such data are essential to constrain the role of fractional crystallization, crustal contamination, and mantle source heterogeneities in the petrogenesis of the alkaline lavas. In this contribution, major and trace element data and Sr–Nd–Pb–O isotope data are reported for primitive alkaline magmas from the Siebengebirge area; these data are used to constrain the mantle source region of these basalts. Major and trace element and Sr–Nd–Pb–O isotope data for more differentiated lavas from the same area are used to highlight the effects of fractional crystallization and crustal contamination in the genesis of these alkaline lavas.

GEOLOGICAL SETTING

The Siebengebirge volcanic field forms part of an east–west-trending belt of Tertiary–Quaternary volcanic fields in central Germany; these include the Eifel, Siebengebirge, Westerwald, Vogelsberg, Hessian Depression, Rhön, Heldburg, and Oberpfalz (Upper Palatinate) (Fig. 1). The trend of these volcanic fields is perpendicular to the main NNE–SSW-trending Rhine graben rift system of Central Europe, which has been interpreted to be the result of Alpine tectonism farther south (e.g. Ziegler, 1992).

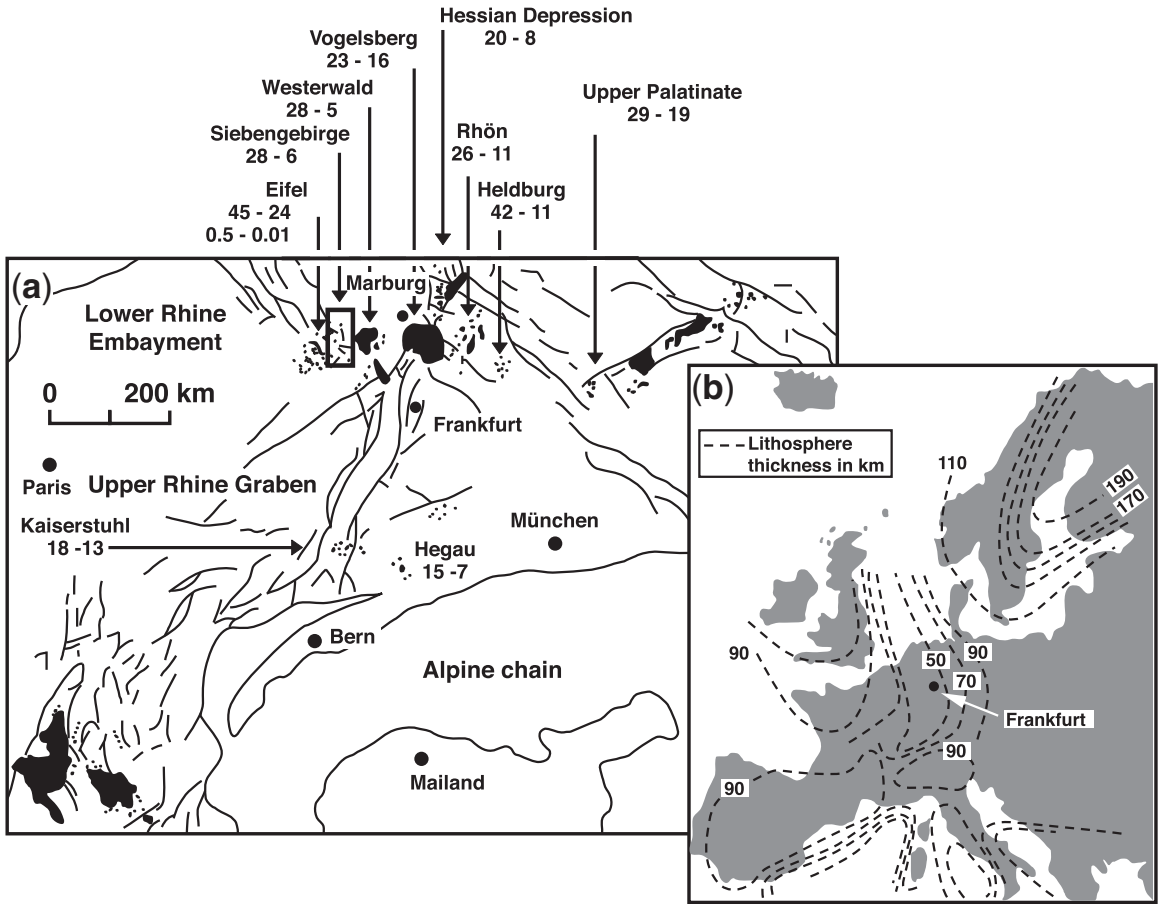

Fig. 1. (a) Distribution of Cenozoic volcanic rocks in Central Europe, modified from Wedepohl *et al.* (1994). Numbers denote K–Ar or Ar–Ar ages compiled from Lippolt (1982) and Wilson & Downes (2006). (b) Contour map of lithospheric thickness in Europe, modified from Wedepohl *et al.* (1994).

In Germany and elsewhere in Central Europe, Tertiary (mainly Miocene to Pliocene) basin development provides evidence for lithospheric extension, although the huge volumes of basaltic rocks in the Vogelsberg area (*c.* 500 km^3) and the Cantal (Massif Central, France) are unlikely to be attributed to continental extension alone. As noted by Wilson & Downes (1991), most of the major volcanic fields are located on uplifted Variscan basement massifs. However, basement uplift is not coeval with rift development, typically starting some 20–40 Myr after the beginning of rifting (Ziegler, 1992). Within Central Germany, although some of the Cenozoic volcanic fields are located mainly on Hercynian fault blocks within the Rhenish Massif (e.g. Eifel, Siebengebirge, Westerwald, Heldburg), Tertiary volcanic activity in the Rhön, the Hessian Depression and the Vogelsberg occurs within graben-like structures that transect the Rhenish Massif. Geophysical data indicate that the Cenozoic rifts of the CEVP are associated with a marked uplift of the Moho discontinuity. The maximum crustal thinning coincides with the trace of the northern Rhine graben although this area has been shown to be largely non-magmatic (Wilson & Patterson, 2001). Crustal thickness beneath the Rhenish Massif is estimated to be between 28 and 32 km (Mengel *et al.*, 1991; Prodehl *et al.*, 1992). Babuska & Plomerová (1988) estimated a lithosphere thickness of 100–140 km prior to the Cenozoic rifting and suggested a present-day depth of less than 60 km for the asthenosphere–lithosphere boundary beneath the Rhenish Massif. More recent estimates (Babuska & Plomerová, 2006), however, indicate a somewhat deeper level for the asthenosphere–lithosphere boundary of about 90 km.

Volcanism within the CEVP spans the entire Cenozoic period (Wilson & Downes, 1991); in the Siebengebirge area it ranged from late Oligocene to early Pliocene (28–6 Ma; Todt & Lippolt, 1980). The Siebengebirge volcanic field has an areal extent of *c.* 1500 km^2 and consists mainly of deeply eroded volcanic plugs and necks. Locally, remnants of lava flows occur. The volcanic activity produced mainly basanites through the entire period between 28 and 6 Ma and rare alkali basalts between 25 and 23 Ma.

Differentiated rocks (trachytes, latites, tephriphonolites and phonotephrites) erupted shortly after the onset of volcanism between 26 and 24 Ma (Vieten *et al.*, 1988). The Hercynian basement through which the magmas erupted consists mainly of greenschist- to amphibolite-facies metapelites, metabasites and orthogneisses of the Mid German Crystalline Rise and is overlain by Palaeozoic (early to late Devonian) limestones and sandstones and Cenozoic sandstones, carbonates and clays (Mengel *et al.*, 1991, and references therein). Information on sample locations is given in Table 1 and as Supplementary Data, Electronic Appendix Table 1 (available for downloading at http://www.petrology.oxfordjournals.org) and the locations are shown in Fig. 2.

ANALYTICAL TECHNIQUES

The data used in this study comprise two datasets. One dataset, collected by Stefan Jung (S.J.), comprises 24 samples covering the entire range of compositions represented by the 66 samples from the other dataset, collected by Klaus Vieten (K.V.). Information for these latter samples can be found as Supplementary Data in the Electronic Appendix. All samples were taken from remnants of lava flows, plugs and necks that geographically cover the entire volcanic field. Whole-rock samples from the dataset collected by S.J. were prepared by crushing in an agate mill to obtain *c.* 250 g of the macroscopically freshest material. Samples collected by K.V. were ground in a tungsten carbide mill. Aliquots were analyzed for major and trace elements on fused lithium-tetraborate glass beads using standard X-ray fluorescence (XRF) techniques (Vogel & Kuipers, 1987) at the Mineralogisch-Petrographisches Institut der Universität Hamburg (S.J.). Loss on ignition (LOI) was determined gravimetrically at 1050°C (Lechler & Desilets, 1987). Trace elements were analysed by inductively coupled plasma mass spectrometry (ICP-MS) at the Universität Bremen. Accuracy was monitored by repeated measurements of international and in-house standards; the results are in good agreement with the recommended values for the international rock standard BCR-1 and BCR-2 given by Govindaraju (1994) (Table 2). Some Pb and all Sr and Nd isotope analyses were carried out at the Institut für Mineralogie at the Universität Münster by thermal ionization mass spectrometry. Strontium and Nd isotopes were determined using a Finnigan Triton® multiple sample, multicollector mass spectrometer operating in the static mode. Lead isotopes on the primitive lavas were measured on a VG 54 multiple sample, multicollector mass spectrometer. Whole-rock chips were leached in 2·5 N HCl for at least 2 h on a hotplate. Subsequently, the samples were washed three times with ultrapure H_2O. After this treatment, the samples were dissolved in concentrated HF and after evaporation redissolved in 2·5 N HCl and 0·6 N HBr and loaded on Teflon® columns filled with DOWEX® AG 1×8 anion exchange resin (100–200 mesh) in chloride form (Mattinson, 1986). The Pb was extracted using conventional HBr–HCl techniques and was loaded on Re single filaments following the H_3PO_4–silica gel method (Cameron *et al.*, 1969). Lead isotopes on the differentiated lavas were measured at the GFZ (Geoforschungszentrum) in Potsdam following the method described by Romer & Hahne (2010). Strontium and REE were separated by using standard cation exchange columns with a DOWEX® AG 50 W-X 12 resin using 2·5 N HCl for Sr and 6 N HCl for the REE. Nd was separated from the other REE by using HDEHP-coated Teflon® columns and 0·12 N HCl. Neodymium isotopes were normalized to $^{146}Nd/^{144}Nd = 0{\cdot}7219$. Repeated measurements of the La Jolla Nd standard gave $^{143}Nd/^{144}Nd = 0{\cdot}511856 \pm 0{\cdot}000003$ (2σ; $n = 4$), which agrees well with the long-term reproducibility of $0{\cdot}511863 \pm 0{\cdot}000003$ during the period. The reproducibility of the Sr standard (NBS 987) is $^{87}Sr/^{86}Sr = 0{\cdot}710203 \pm 0{\cdot}000009$ (2σ; $n = 4$) which is similar to the long-term reproducibility of $0{\cdot}710207 \pm 0{\cdot}000009$. Fractionation was corrected to $^{86}Sr/^{88}Sr = 0{\cdot}1194$. Lead analyses in Münster were corrected for mass fractionation by a factor of 0·11% per atomic mass unit (a.m.u.). In Potsdam, mass fractionation was corrected with 0·06% per a.m.u. The reproducibility of the standard NBS 982 was estimated to be 0·064%, 0·068% and 0·071% for $^{206}Pb/^{204}Pb$, $^{207}Pb/^{204}Pb$ and $^{208}Pb/^{204}Pb$, respectively. The total procedure blank is <100 pg Pb during this study and is therefore considered negligible. Isotope data are given in Table 3.

The other dataset (66 samples, Supplementary Data, Electronic Appendix Table 2), compiled by K.V. during recent decades, comprises major elements and some trace elements (Rb, Ba, Sr, Zr, Ni, Co, Cr, V) analysed by XRF at the University of Bonn with standard techniques (Vogel & Kuipers, 1987). For some samples, REE concentrations were analysed by inductively coupled plasma atomic emission spectrometry (ICP-AES) following separation of the matrix elements by ion exchange (Heinrichs & Herrmann, 1990) at the Institut für Mineralogie, Petrologie und Kristallographie (Universität Marburg). Accuracy was monitored by repeated measurements against an in-house standard (basalt BB, Engelhardt, 1990) which was calibrated against international rock standards (Jung *et al.*, 2006). Strontium isotope analyses for some samples from this dataset were carried out at the Universität Tübingen and followed the procedure outlined by Hegner *et al.* (1995). Oxygen isotope analyses on whole-rock samples and some mineral separates were performed at the Universität Bonn on 8–10 mg aliquots of powdered whole-rock samples or minerals, using purified fluorine for oxygen extraction, followed by conversion to CO_2 (Clayton & Mayeda, 1963). $^{18}O/^{16}O$ measurements were made on a VG-Isogas® SIRA-9 triple-collector mass spectrometer.

Table 1: Sample number, localities and short petrographic description of the Siebengebirge volcanic rocks

Sample no.	Locality	No. in Fig. 1	Map no.	Rechtswert	Hochwert	Longitude	Latitude	Rock type	Petrography
SG 4	Broderkronsberg	1	5309	259095	561350	7°17′10·27″	50°39′4·40″	AOB	fine grained, <20% phen of cpx, pl, minor ol
SG 13	Hupperichsberg	2	5309	259090	561262	7°17′6·95″	50°38′35·96″	Mugearite	fine grained, <20% phen of cpx, pl. Altered amph, flow texture
SG 11	Petersberg	4	5309	258545	561744	7°12′33·61″	50°41′14·89″	AOB	fine-grained, <10% phen of ol and cpx, groundmass cpx and pl
SG 18	Stenzelberg	5	5309	258666	561800	7°13′35·71″	50°41′32·37″	Mugearite	fine-grained, <20% of amph, cpx and pl. Amph altered
SG 5	Ölberg	6	5309	258829	561701	7°14′57·90″	50°40′59·45″	Benmoreite	fine-grained, <20% phen of amph, cpx, bt, pl, flow texture
SG 6	Ölberg	6	5309	258829	561701	7°14′57·90″	50°40′59·45″	AOB	fine-grained basalt, <10% phen of cpx and ol, ol xenocrysts, abundant pl, flow texture
SG 15	Himmerich	9	5309	259076	561283	7°17′0·01″	50°38′42·83″	Mugearite	fine-grained mugearite, <10% phen of pl and cpx, flow texture
SG 14	Mittelberg	10	5309	259035	561251	7°16′38·86″	50°38′32·71″	Mugearite	fine-grained mugearite, <20% phen of cpx, pl. Altered amph, flow texture
SG 19	Himberg	11	5309	259240	561320	7°18′23·80″	50°38′53·88″	Basanite	glassy basalt, <15% phen of ol and cpx
SG 3	Asberg	12	5309	259199	561097	7°18′0·94″	50°37′41·95″	Basanite	fine-grained basalt, <10% phen of ol and cpx, groundmass pl
SG 2	Meerberg	13	5309	259190	560895	7°17′54·56″	50°36′36·64″	Basanite	fine-grained basalt, <15% phen of ol and cpx, ol skeletal and altered, groundmass pl
SG 8	Löwenburg	15	5309	258850	561500	7°15′6·86″	50°39′54·30″	Tephrite	medium-grained basalt, 10% ol, 30% cpx, 60% pl
SG 10	Wolkenburg	16	5309	258601	561535	7°13′0·38″	50°40′6·97″	Trachyte	fine-grained trachyte, <20% phen of bt, pl, ttn, kfs
SG 9	Drachenfels	17	5309	258566	561483	7°12′42·13″	50°39′50·33″	Trachyte	fine-grained trachyte, <20% phen of kfs, bt, pl, cpx, flow texture
SG 16	Schellkopf	18	5309	258972	561459	7°16′8·62″	50°39′40·36″	Basanite	glassy basalt, <15% phen of cpx and ol, mantle and crustal xenoliths, green-core cpx
SG 17	Gr. Weilberg	20	5309	258630	561880	7°13′18·05″	50°41′58·45″	AOB	fine-grained basalt, <15% phen of cpx and ol, glassy groundmass, flow texture
SG 7	Lohrberg	21	5309	258835	561587	7°14′59·97″	50°40′22·53″	Benmoreite	fine-grained benmoreite, <20% phen of bt, pl, ttn, cpx
SG 21	Stuxenberg	25	5209	259315	562110	7°19′9·13″	50°43′9·07″	Basanite	fine-grained basalt, <20% phen of ol, cpx, ol altered
SG 20	Gr. Scharfenberg	26	5209	258750	562000	7°14′20·21″	50°42′36·63″	AOB	fine-grained basalt, <20% phen of cpx, rare skeletal ol, cpx xenocrysts
SG 23	Priesterberg	27	5210	259714	562030	7°22′31·74″	50°42′40·83″	Basanite	glassy basalt, <15% phen of ol and cpx, groundmass cpx, altered skeletal ol
SG 22	Eulenberg	28	5210	259640	562080	7°21′54·50″	50°42′57·45″	Basanite	glassy basalt, <20% phen of ol and cpx, green-core cpx, minor pl
SG 24	Stein	29	5210	260379	563186	7°28′22·34″	50°48′50·71″	Basanite	fine-grained basalt, <20% phen of ol and cpx, groundmass pl, green-core cpx
SG 12	Bertenauer Kopf	33	5310	260172	560970	7°26′14·65″	50°36′55·05″	Basanite	glassy basalt, <15% phen of ol and cpx, groundmass cpx, altered skeletal ol
SG 1	Fernthal	34	5310	260160	560833	7°26′7·19″	50°36′10·79″	Basanite	fine-grained basalt, <10% phen of cpx and ol, glassy groundmass, green-core cpx

Hochwert and Rechtswert indicate position in the German Gauss–Krüger coordinate system. Sample localities shown in Fig. 1. phen, phenocryst; cpx, clinopyroxene; pl, plagioclase; ol, olivine; hbl, hornblende; bt, biotite; ttn, titanite.

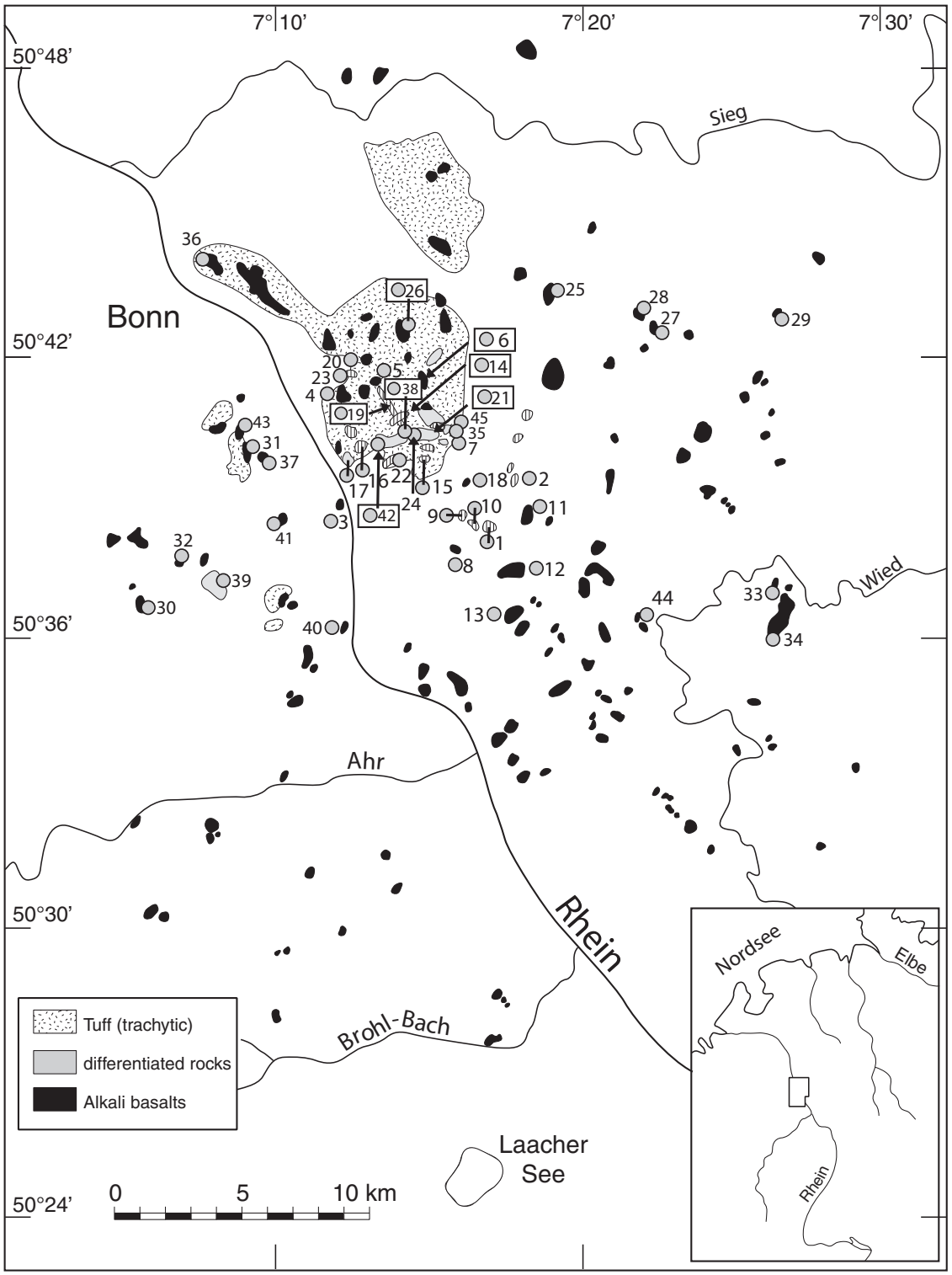

Fig. 2. Location of the volcanic outcrops within the Siebengebirge and sample sites (grey circles). Inset shows the location of the Siebengebirge area within Central Germany. Sample locations given in Table 1.

Table 2: Major and trace elements of Siebengebirge lavas

Rock type:	Basanite	Basanite	Basanite	Basanite	Basanite	Basanite	Basanite
Sample no.:	SG 2	SG 12	SG 23	SG 21	SG 1	SG 3	SG 16
Locality:	13	33	27	25	34	12	18
SiO_2	44·73	42·49	41·95	40·33	42·16	42·87	42·97
TiO_2	2·60	2·52	2·10	2·46	2·36	2·26	2·09
Al_2O_3	13·14	12·75	11·36	13·08	11·84	12·50	11·64
Fe_2O_3	12·17	12·40	12·98	14·34	12·59	12·73	11·69
MnO	0·18	0·21	0·22	0·26	0·20	0·20	0·19
MgO	10·03	11·64	14·00	7·67	13·69	11·48	14·94
CaO	9·78	11·50	10·15	11·47	11·35	9·87	9·89
Na_2O	2·54	3·37	2·81	3·62	2·70	2·64	2·67
K_2O	1·60	0·50	1·31	0·92	1·30	1·26	1·38
P_2O_5	0·47	0·53	0·59	0·85	0·50	0·49	0·58
LOI	2·31	2·27	2·10	3·94	1·30	1·94	1·40
Sum	99·55	100·18	99·57	98·94	99·99	98·24	99·44
Li	15·3	9·2	6·5	6·7	9·7	11·5	7·8
Sc	23·9	30·2	23·0	22·5	33·4	21·3	22·9
V	229	283	194	237	280	224	213
Cr	319	463	596	241	566	337	513
Co	70·8	53·1	30·3	51·5	58·3	58·8	56·7
Ni	217	212	442	166	286	270	438
Cu	56·7	67·1	27·4	55·0	70·2	90·7	49·1
Zn	148	97	167	113	167	125	127
Ga	19·8	16·0	11·9	18·8	16·3	17·3	15·7
Rb	48·4	70·7	30·4	37·8	47·2	32·2	35·9
Sr	684	710	726	1061	660	708	783
Y	27·7	23·6	22·3	28·0	23·1	24·9	22·5
Zr	250	216	213	237	203	216	225
Nb	58	89	83	101	86	64	87
Cs	0·95	0·94	0·64	11·57	1·56	2·48	0·85
Ba	496	684	508	862	628	654	593
La	39·2	59·9	56·9	80·7	57·5	47·4	63·4
Ce	78·8	109	104	142	107	89·1	115
Pr	9·5	12·2	11·4	15·5	12·1	10·2	12·6
Nd	37·8	44·9	41·6	54·9	44·1	38·4	45·5
Sm	7·3	7·6	7·2	9·2	7·6	7·2	7·7
Eu	2·27	2·29	2·22	2·81	2·27	2·23	2·35
Gd	6·3	6·3	5·9	7·5	6·2	6·2	6·4
Tb	0·9	0·9	0·8	1·1	0·9	0·9	0·9
Dy	4·9	4·8	4·5	5·4	4·8	4·8	4·8
Ho	0·9	0·9	0·8	1·0	0·9	0·9	0·8
Er	2·3	2·3	2·1	2·5	2·3	2·3	2·2
Tm	0·3	0·31	0·28	0·33	0·32	0·31	0·3
Yb	1·8	1·9	1·7	2·0	1·9	1·9	1·8
Lu	0·25	0·27	0·24	0·29	0·26	0·26	0·25
Hf	5·20	4·40	4·20	4·90	4·40	4·50	4·80
Ta	3·20	5·00	4·60	5·90	6·00	3·30	4·70
Pb	5·45	3·75	4·30	4·44	3·93	4·44	4·53
Th	5·00	8·20	8·50	8·30	7·70	6·50	8·70
U	1·40	1·51	2·20	2·10	2·00	1·80	2·30

(continued)

Table 2: Continued

Rock type:	Basanite	Basanite	Basanite	AOB	AOB	AOB	AOB
Sample no.:	SG 19	SG 22	SG 24	SG 4	SG 6	SG 11	SG 17
Locality:	11	28	29	1	6	4	20
SiO_2	43·49	43·35	43·12	47·55	45·24	45·15	45·89
TiO_2	2·19	2·07	2·19	1·87	2·10	2·12	2·25
Al_2O_3	12·59	11·63	13·16	14·07	13·37	13·11	14·50
Fe_2O_3	12·17	11·83	11·44	11·32	11·58	13·01	11·51
MnO	0·18	0·18	0·17	0·20	0·18	0·20	0·19
MgO	11·98	14·92	11·82	8·61	9·97	9·62	7·89
CaO	10·10	9·71	10·57	9·61	10·00	9·67	9·97
Na_2O	2·27	2·67	2·53	2·86	2·98	2·84	2·74
K_2O	1·40	0·84	0·84	1·22	1·36	1·25	1·34
P_2O_5	0·51	0·58	0·46	0·37	0·43	0·48	0·42
LOI	2·05	2·47	2·66	1·78	1·77	1·58	2·43
Sum	98·93	100·25	98·96	99·46	98·98	99·03	99·13
Li	8·7	9·9	8·1	9·0	12·7	10·6	6·5
Sc	25·7	22·4	28·7	22·1	26·0	23·7	24·7
V	227	208	246	189	228	207	225
Cr	452	479	354	288	289	254	208
Co	55·0	55·1	53·5	45·6	51·1	55·3	45·0
Ni	323	451	243	194	200	204	139
Cu	62·6	54·7	67·4	64·5	55·9	54·2	60·2
Zn	140	181	128	153	123	140	103
Ga	18·0	15·5	16·7	17·9	17·8	18·8	18·9
Rb	45·9	43·3	42·4	42·0	38·4	39·7	40·7
Sr	724	746	627	1136	731	776	1234
Y	22·3	22·5	20·9	26·7	26·5	26·3	23·3
Zr	237	207	182	240	223	235	232
Nb	79	76	76	68	72	68	62
Cs	0·68	1·18	0·91	1·06	0·54	0·68	0·51
Ba	816	567	533	1573	673	828	758
La	47·7	53·9	42·3	58·2	52·2	59·2	45·8
Ce	89·7	98·6	77·1	101	94·2	108	84·2
Pr	10·4	11·1	8·69	10·8	10·5	12·0	9·43
Nd	38·4	40·9	32·3	38·4	38·7	44·1	35·2
Sm	6·94	7·13	6·02	6·93	7·31	8·01	6·62
Eu	2·13	2·18	1·84	2·18	2·22	2·45	2·05
Gd	6·02	5·93	5·11	6·03	6·24	7·04	5·71
Tb	0·91	0·92	0·84	0·93	0·91	1·02	0·83
Dy	4·73	4·51	4·12	5·03	5·04	5·54	4·61
Ho	0·81	0·83	0·72	0·93	0·94	1·02	0·82
Er	2·12	2·13	2·02	2·51	2·53	2·52	2·23
Tm	0·28	0·28	0·27	0·35	0·33	0·34	0·31
Yb	1·72	1·73	1·61	2·13	2·04	2·03	1·81
Lu	0·24	0·26	0·25	0·30	0·29	0·29	0·27
Hf	4·90	4·30	4·30	4·90	4·50	4·90	4·70
Ta	4·20	4·20	4·20	4·00	3·90	3·30	3·50
Pb	4·30	4·73	3·41	5·34	5·46	3·94	4·07
Th	6·90	7·60	6·40	6·90	7·40	7·00	6·50
U	1·80	1·90	1·60	1·90	1·70	1·80	1·60

(continued)

Table 2: Continued

Rock type:	AOB	Tephrite	Mugearite	Mugearite	Mugearite	Mugearite	Benmoreite
Sample no.:	SG 20	SG 8	SG 13	SG 14	SG 15	SG 18	SG 5
Locality:	26	15	2	10	9	5	6
SiO_2	45·95	48·41	52·77	53·61	53·45	55·30	57·92
SiO_2	45·95	48·41	52·77	53·61	53·45	55·30	57·92
TiO_2	2·32	2·30	1·99	1·81	1·84	1·78	1·41
Al_2O_3	13·84	15·32	18·13	18·13	18·08	17·04	17·41
Fe_2O_3	12·89	9·69	7·33	7·07	6·91	7·10	5·30
MnO	0·19	0·17	0·17	0·20	0·19	0·16	0·10
MgO	8·26	6·47	2·26	2·21	2·04	2·07	1·83
CaO	10·14	8·63	5·86	6·23	6·14	5·81	3·75
Na_2O	3·13	4·53	3·95	4·17	4·03	3·89	3·98
K_2O	0·58	2·67	3·92	4·21	4·02	3·80	4·05
P_2O_5	0·45	0·69	0·50	0·46	0·48	0·43	0·32
LOI	1·51	1·19	2·72	1·80	2·59	2·28	3·42
Sum	99·26	100·07	99·60	99·90	99·77	99·66	99·49
Li	8·1	22·4	16·4	28·9	27·4	21·7	29·8
Sc	24·9	20·2	10·5	8·2	9·4	12·7	10·4
V	213	199	210	178	193	188	141
Cr	228	170	16·7	12·1	9·7	22·2	18·9
Co	48·6	32·1	22·2	14·3	15·1	16·0	12·5
Ni	153	81·3	37·0	11·1	6·8	10·7	12·9
Cu	55·5	42·4	16·1	13·3	13·0	27·1	19·1
Zn	151	127	103	109	160	95	122
Ga	18·7	22·6	24·0	23·6	24·5	23·2	23·8
Rb	13·5	78·7	102·7	105·2	119·3	118·8	132·0
Sr	587	1053	798	835	868	748	536
Y	25·2	24·8	27·5	28·7	31·9	29·8	29·9
Zr	174	418	439	456	468	416	424
Nb	54	100	84	95	97	65	74
Cs	0·63	2·79	1·54	2·24	1·58	2·30	2·28
Ba	470	780	962	965	837	743	833
La	44·2	82·8	74·2	79·3	82·7	69·5	61·1
Ce	79·4	152	139	143	149	136	116
Pr	9·22	16·5	14·5	15·0	15·9	14·9	12·8
Nd	35·2	58·9	50·9	52·6	55·7	53·5	45·7
Sm	6·84	9·51	9·31	9·24	9·95	9·30	8·43
Eu	2·16	2·67	2·59	2·53	2·64	2·60	2·29
Gd	6·03	7·21	7·21	7·36	7·95	7·79	6·90
Tb	0·92	1·02	0·99	0·98	1·04	1·01	0·90
Dy	4·71	4·91	5·52	5·59	5·96	5·96	5·49
Ho	0·92	0·93	1·01	1·07	1·13	1·10	1·03
Er	2·33	2·32	2·82	2·87	3·10	2·93	2·94
Tm	0·31	0·31	0·39	0·43	0·44	0·40	0·43
Yb	1·64	1·82	2·47	2·53	2·72	2·57	2·51
Lu	0·22	0·25	0·37	0·41	0·43	0·38	0·40
Hf	3·90	7·80	8·00	8·30	8·50	8·20	8·40
Ta	3·10	5·50	4·80	5·20	5·50	3·80	4·20
Pb	3·06	8·07	10·23	16·52	8·93	10·89	20·97
Th	4·50	14·40	15·30	15·90	21·00	16·40	17·40
U	1·10	4·40	4·60	4·40	4·40	4·50	5·20

(continued)

Table 2: Contiued

Rock type:	Benmoreite	Trachyte	Trachyte	Standard	Standard
Sample no.:	SG 7	SG 9	SG 10	BCR-2	BCR-2
Locality:	21	17	16	measured	rec. values
SiO_2	60·33	61·90	62·79	53·98	54·11
SiO_2	60·33	61·90	62·79	53·98	54·11
TiO_2	0·93	0·85	0·69	2·27	2·24
Al_2O_3	18·14	17·21	17·43	13·42	13·64
Fe_2O_3	4·34	3·91	3·39	13·67	13·41
MnO	0·14	0·13	0·13	0·19	0·18
MgO	1·06	1·08	0·90	3·52	3·48
CaO	3·61	3·54	2·71	7·03	6·95
Na_2O	4·77	4·81	4·59	3·12	3·27
K_2O	4·03	4·18	4·36	1·75	1·69
P_2O_5	0·27	0·27	0·21	0·35	0·36
LOI	1·94	1·69	2·38	0·69	1·59
Sum	99·56	99·57	99·58	99·99	100·92
Li	34·4	36·3	35·7	9·2	9
Sc	7·2	5·3	4·8	34·7	33
V	86	68	57	444	416
Cr	11·5	6·8	9·8	15·9	18
Co	8·32	6·16	5·87	37·6	37
Ni	8·3	4·2	5·5	11·8	13
Cu	11·7	9·15	10·9	16·3	19
Zn	86	99	108	132	127
Ga	24·8	23·8	24·1	22·1	23
Rb	142·8	150·4	149·3	47·0	48
Sr	661	611	549	341	346
Y	23·4	21·6	17·2	33·6	37
Zr	413	403	338	187	188
Nb	72	67	50	12	14
Cs	1·92	1·98	2·69	1·11	1·1
Ba	857	676	762	662	683
La	66·7	63·7	52·6	24·3	25
Ce	121	113	90·2	50·8	53
Pr	11·8	11·2	8·91	6·53	6·8
Nd	40·2	37·9	30·0	27·3	28
Sm	7·11	6·54	5·25	6·49	6·7
Eu	1·87	1·72	1·35	1·94	2·0
Gd	5·59	5·38	4·33	6·76	6·8
Tb	0·75	0·72	0·56	1·02	1·07
Dy	4·30	4·08	3·27	6·30	6·34
Ho	0·81	0·77	0·62	1·27	1·33
Er	2·34	2·24	1·80	3·55	3·63
Tm	0·34	0·31	0·25	0·51	0·54
Yb	2·13	1·96	1·61	3·23	3·5
Lu	0·31	0·28	0·23	0·51	0·51
Hf	7·80	8·00	7·10	5·02	4·8
Ta	4·10	3·70	3·00	0·85	0·81
Pb	14·22	18·48	15·01	9·42	11
Th	18·80	20·40	20·30	5·46	6·2
U	5·00	6·00	4·70	1·51	1·69

LOI, loss on ignition. Major elements in wt %, trace elements in ppm.

Table 3: Sr, Nd and Pb isotope composition of Siebengebirge lavas

Sample	Rock type	$^{87}Sr/^{86}Sr(m)$	$^{87}Rb/^{86}Sr$	$^{87}Sr/^{86}Sr(i)$	$^{143}Nd/^{144}Nd(m)$	$^{147}Sm/^{144}Nd$	$^{143}Nd/^{144}Nd(i)$	εNd	$^{206}Pb/^{204}Pb(m)$	$^{207}Pb/^{204}Pb(m)$	$^{208}Pb/^{204}Pb(m)$	$^{206}Pb/^{204}Pb(i)$	$^{207}Pb/^{204}Pb(i)$	$^{208}Pb/^{204}Pb(i)$
SG 2	Bas	0·703406(12)	0·205	0·703325	0·512865(11)	0·122	0·512843	+4·7	19·58	15·63	39·38	19·51	15·63	39·29
SG 12	Bas	0·703624(10)	0·288	0·703509	0·512827(09)	0·110	0·512807	+4·0	n.a.	n.a.	n.a.	n.a.	n.a.	n.a.
SG 23	Bas	0·703403(09)	0·121	0·703355	0·512847(10)	0·121	0·512825	+4·3	19·50	15·62	39·36	19·35	15·61	39·18
SG 21	Bas	0·703412(11)	0·103	0·703371	0·512855(12)	0·109	0·512835	+4·5	n.a.	n.a.	n.a.	n.a.	n.a.	n.a.
SG 1	Bas	0·703644(13)	0·207	0·703562	0·512826(09)	0·116	0·512805	+4·0	19·67	15·63	39·44	19·53	15·62	39·26
SG 3	Bas	0·703601(10)	0·132	0·703549	0·512835(10)	0·121	0·512813	+4·1	19·56	15·61	39·33	19·49	15·61	39·25
SG 16	Bas	0·703408(09)	0·133	0·703355	0·512850(11)	0·114	0·512829	+4·4	n.a.	n.a.	n.a.	n.a.	n.a.	n.a.
SG 19	Bas	0·703480(10)	0·184	0·703407	0·512843(12)	0·120	0·512821	+4·3	19·76	15·63	39·60	19·64	15·62	39·49
SG 22	Bas	0·703418(11)	0·168	0·703351	0·512843(10)	0·115	0·512822	+4·3	19·70	15·68	39·61	19·59	15·67	39·46
SG 24	Bas	0·703520(09)	0·196	0·703442	0·512836(10)	0·120	0·512814	+4·1	19·61	15·62	39·43	19·49	15·62	39·43
SG 17	AOB	0·703568(11)	0·096	0·703530	0·512822(09)	0·125	0·512799	+3·8	19·46	15·64	39·36	19·44	15·62	39·20
SG 4	AOB	0·703488(12)	0·107	0·703445	0·512836(11)	0·115	0·512815	+4·2	19·02	15·59	38·84	18·97	15·59	38·78
SG 6	AOB	0·703566(11)	0·152	0·703506	0·512827(09)	0·120	0·512805	+4·0	19·84	15·65	39·75	19·75	15·65	39·66
SG 11	AOB	0·703463(13)	0·148	0·703404	0·512853(11)	0·116	0·512832	+4·5	n.a.	n.a.	n.a.	n.a.	n.a.	n.a.
SG 20	AOB	0·703395(11)	0·066	0·703369	0·512867(12)	0·130	0·512843	+4·7	n.a.	n.a.	n.a.	n.a.	n.a.	n.a.
SG 8	Teph	0·704341(09)	0·216	0·704255	0·512747(11)	0·112	0·512726	+2·4	19·45	15·64	39·28	19·31	15·63	39·13
SG 13	Mug	0·704046(13)	0·373	0·703898	0·512727(09)	0·110	0·512707	+2·0	19·44	15·67	39·37	19·33	15·67	39·25
SG 14	Mug	0·704636(13)	0·365	0·704491	0·512731(10)	0·106	0·512712	+2·1	19·46	15·67	39·36	19·39	15·67	39·28
SG 15	Mug	0·704680(11)	0·398	0·704522	0·512726(09)	0·108	0·512706	+2·0	19·43	15·66	39·33	19·31	15·66	39·13
SG 18	Mug	0·705397(11)	0·460	0·705214	0·512664(10)	0·105	0·512645	+0·8	19·32	15·68	39·35	19·22	15·68	39·22
SG 5	Ben	0·705845(12)	0·713	0·705562	0·512654(09)	0·111	0·512634	+0·6	19·38	15·68	39·37	19·31	15·67	39·30
SG 7	Ben	0·705642(13)	0·625	0·705393	0·512614(10)	0·107	0·512594	−0·1	19·35	15·67	39·33	19·26	15·67	39·22
SG 9	Tr	0·705624(11)	0·713	0·705340	0·512657(10)	0·104	0·512638	+0·7	19·37	15·67	39·37	19·29	15·66	39·27
SG 10	Tr	0·706002(12)	0·787	0·705689	0·512610(11)	0·106	0·512591	−0·2	19·34	15·66	39·31	19·26	15·65	39·20

Numbers in parentheses are 2σ in-run deviations of the measurements. Initial Sr, Nd and Pb isotope compositions were recalculated using Rb, Sr, Sm, Nd, U, Pb and Th concentrations from Table 3 and an age of 28 Ma. (m), measured; (i), initial. Bas, basanite; AOB, alkali olivine basalt; Teph, tephrite; Mug, mugearite; Ben, benmoreite; Tr, trachyte. n.a., not analysed.

Analytical uncertainties are <0·2‰. Strontium isotope data and whole-rock and mineral $\delta^{18}O$ values are given as Supplementary Data in Electronic Appendix Table 3.

RESULTS

Petrography and mineralogy of the Siebengebirge lavas

All basaltic samples are porphyritic and contain partly altered olivine and clinopyroxene phenocrysts. Usually, the majority of the olivine and clinopyroxene phenocrysts have grain sizes of *c.* 0·5–2 mm and 0·2–5 mm, respectively and the samples containing such phenocrysts do not appear to be accumulative. Rare olivines in some basanites have a mosaic texture and incipient undulose extinction. They probably represent entrained material from disintegrated peridotite xenoliths. The dominant olivines within the basanites and alkali basalts are euhedral phenocrysts with sharply defined crystal edges. Sometimes the olivines are more skeletal, which is indicative of fast cooling. Some olivines show evidence of marginal resorption, re-entrants and internal cavities, which can be interpreted as a disequilibrium feature. Zoned clinopyroxenes are generally composed of a subhedral to anhedral colourless to pale brown core and a darker brown, slightly pleochroic mantle. In some samples, clinopyroxenes with an olive green to light green core, a colourless to pale brown mantle and a dark brown rim occur in addition to the clinopyroxenes described above (e.g. Duda & Schmincke, 1985; Jung *et al.*, 2006). Some basanites and some of the more differentiated rocks contain optically homogeneous, unzoned brown amphibole with a grain size of between 1 and 5 mm. These hornblende crystals are usually surrounded by a thick opacitized rim or are completely altered. Plagioclase is common only in some alkali basalts and in the more differentiated rocks and is generally unzoned. Rare large plagioclase crystals show the development of K-feldspar-rich rims. More evolved rocks (mostly latites and trachytes) contain hornblende in addition to clinopyroxene and plagioclase or (for trachytes) alkali feldspar phenocrysts in a groundmass that predominantly consists of plagioclase. Clinopyroxene occurs as Ti-augite or aegirine–augite, and biotite together with titanite is common in the more evolved rock types. Additional information on the mineralogy of the various rock types has been given by Vieten *et al.* (1988). Details on the petrography of the samples are given as Supplementary Data in Electronic Appendix Table 1.

Geochemical composition of the Siebengebirge lavas

The mafic volcanic rocks from the Siebengebirge area are mostly relatively primitive basanites and alkali basalts and mugearites, benmoreites and trachytes, according to the total-alkali vs SiO_2 classification scheme of Le Bas *et al.* (1986) (Table 2; Fig. 3). For the basanites and alkali basalts, MgO, CaO, $FeO_{(total)}$ and TiO_2 decrease, whereas K_2O and Al_2O_3 increase with increasing SiO_2 (Fig. 3). Na_2O shows considerable scatter among the basanites and alkali basalts. For the evolved rocks, TiO_2, MgO, CaO and $FeO_{(total)}$ decrease with increasing SiO_2, whereas K_2O and Na_2O increase (Fig. 3). Al_2O_3 increases until ~56 wt % SiO_2 and than stays rather constant until ~64 wt % SiO_2. Additional major element data are plotted in Fig. 1 of the Supplementary Data. It should be noted that the nomenclature adopted here is slightly different and follows that given by Vieten *et al.* (1988).

Trace element data are reported in Table 2 and plotted as a function of SiO_2 (wt %) in Fig. 4. Additional trace element data are plotted in Fig. 2 of the Supplementary Data in the Electronic Appendix. The most interesting feature is the strong overlap in compatible trace element abundances for basanites and alkali basalts. Most basanites and the alkali basalts have Ni, Cr and Co contents that approach the values commonly assumed for primary magmas (e.g. Frey *et al.*, 1978). Ni contents above 300 ppm and Cr contents higher than 500 ppm are probably due to contamination with spinel peridotite xenoliths.

For the incompatible trace elements, La and Zr abundances show strong overlap for basanites and the alkali basalts (Fig. 4), whereas Nb abundances are higher in the basanites relative to the alkali basalts. Consequently, ratios of incompatible trace elements (La/Nb, Zr/Nb, Ba/La, Ba/Nb; Fig. 5) show some overlap for basanites and alkali basalts. Most of the differentiated rocks have higher Zr/Nb and La/Nb ratios, whereas Ba/Nb and Ba/La ratios show nearly complete overlap with the basanites and alkali basalts. The Rb/Nb and K/Nb ratios are positively correlated with SiO_2 and the basanites have similar Rb/Nb and K/Nb ratios to the alkali basalts. The differentiated rocks have the highest Rb/Nb and K/Nb ratios.

Basanites and alkali basalts have light REE (LREE)-enriched REE patterns with a strong enrichment of LREE over heavy REE (HREE). The differentiated rocks have similar REE patterns (Fig. 6). Some samples have a pronounced depletion in middle REE (MREE) (Supplementary Data, Electronic Appendix, Fig. 3). Basanites and alkali basalts show strong enrichment of highly incompatible and moderately incompatible trace elements; K and Rb are depleted relative to elements with similar incompatibility (Fig. 7). Apart from these anomalies, primitive mantle-normalized concentrations increase with increasing incompatibility (Fig. 7).

The Siebengebirge lavas show a negative correlation of Ce/Pb and Nb/U ratios with SiO_2 (Fig. 8). Most of the basanites and alkali basalts have Ce/Pb ratios of 25 ± 5 [with the exceptions of samples SG 2 (Ce/Pb 15), SG 3 (Ce/Pb 11), SG 4 (Ce/Pb 9) and SG 6 (Ce/Pb 16)]

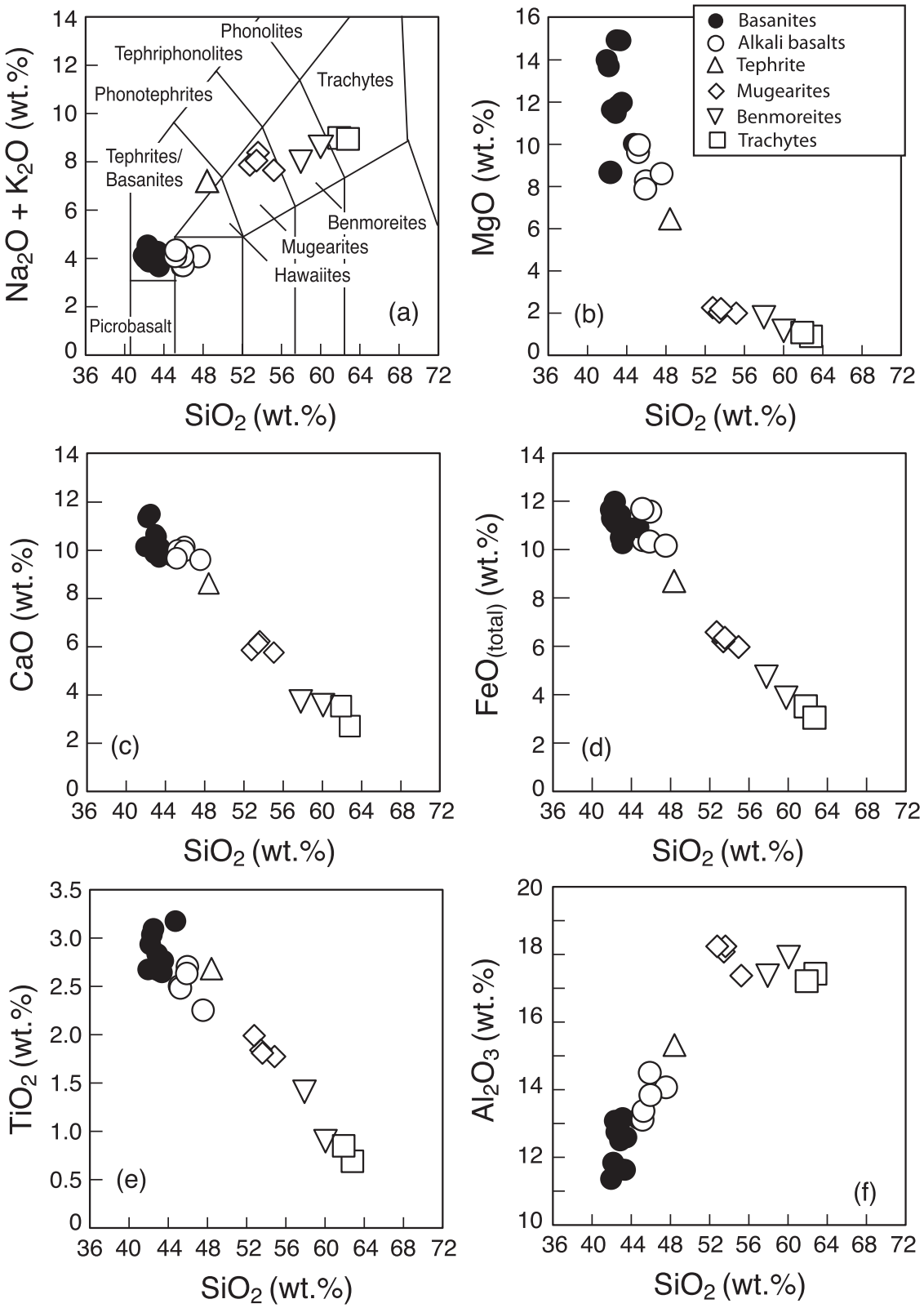

Fig. 3. (a) Total alkalis–silica diagram (Le Bas *et al.*, 1986; Le Maitre *et al.*, 2002), (b) MgO, (c) CaO, (d) FeO(total), (e) TiO_2, and (f) Al_2O_3 vs SiO_2 for the Siebengebirge lavas.

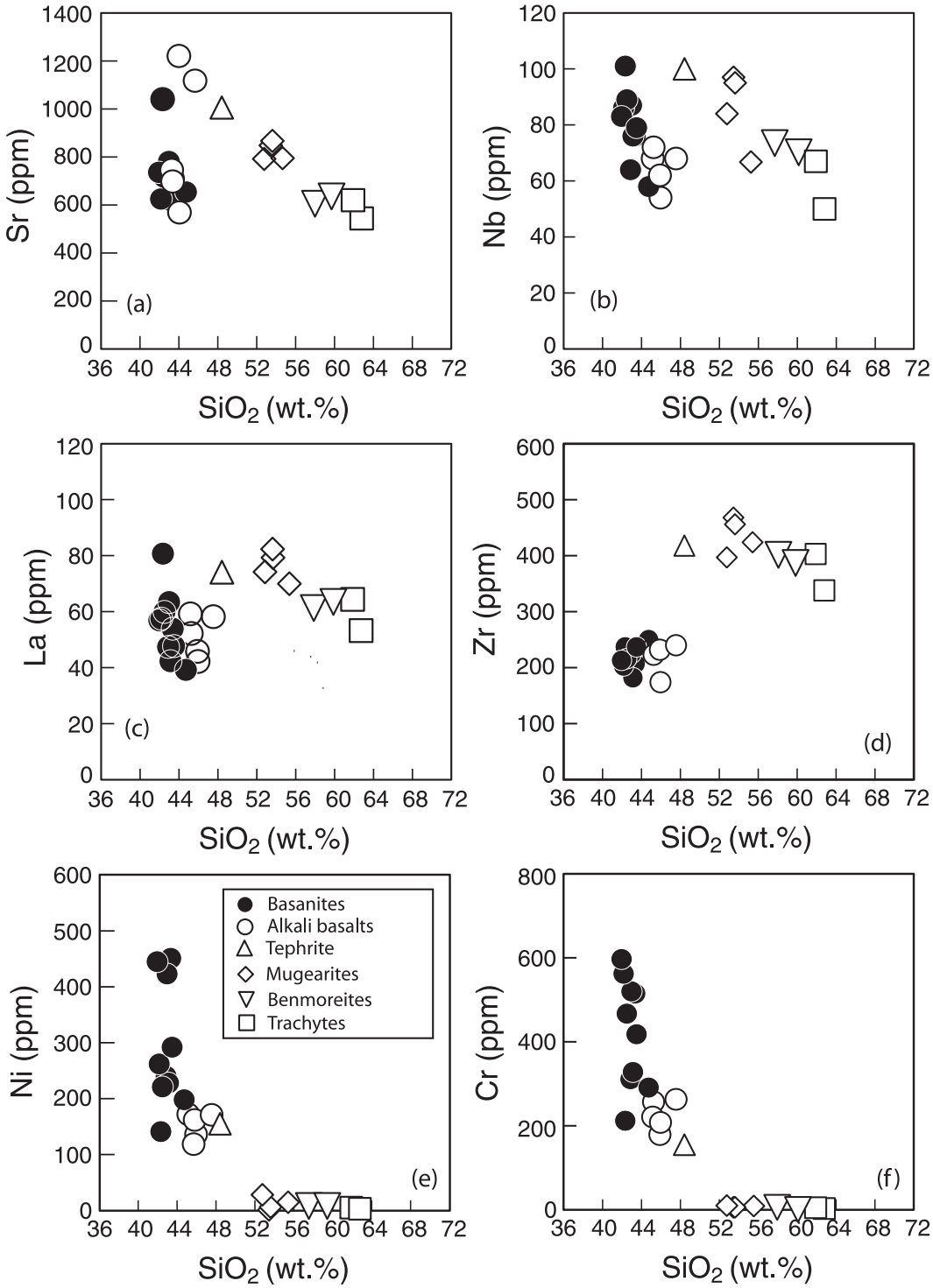

Fig. 4. (a) Sr (in ppm) vs SiO_2, (b) Nb (in ppm) vs SiO_2, (c) La (in ppm) vs SiO_2; (d) Zr (in ppm) vs SiO_2; (e) Ni (in ppm) vs SiO_2; (f) Cr (in ppm) vs SiO_2 for the Siebengebirge lavas.

and Nb/U ratios of 47 ± 10; resembling the ratios for oceanic basalts (Hofmann *et al.*, 1986; Fig. 8). The evolved lavas have significantly lower Ce/Pb (16–5) and Nb/U (24–11) ratios approaching the values for typical crustal rocks or average lower crust (Ce/Pb 5; Nb/U 25; Kemp & Hawkesworth, 2004; Rudnick & Gao, 2004) and some lower crustal xenoliths from the Rhenish Shield (Sachs & Hansteen, 2000).

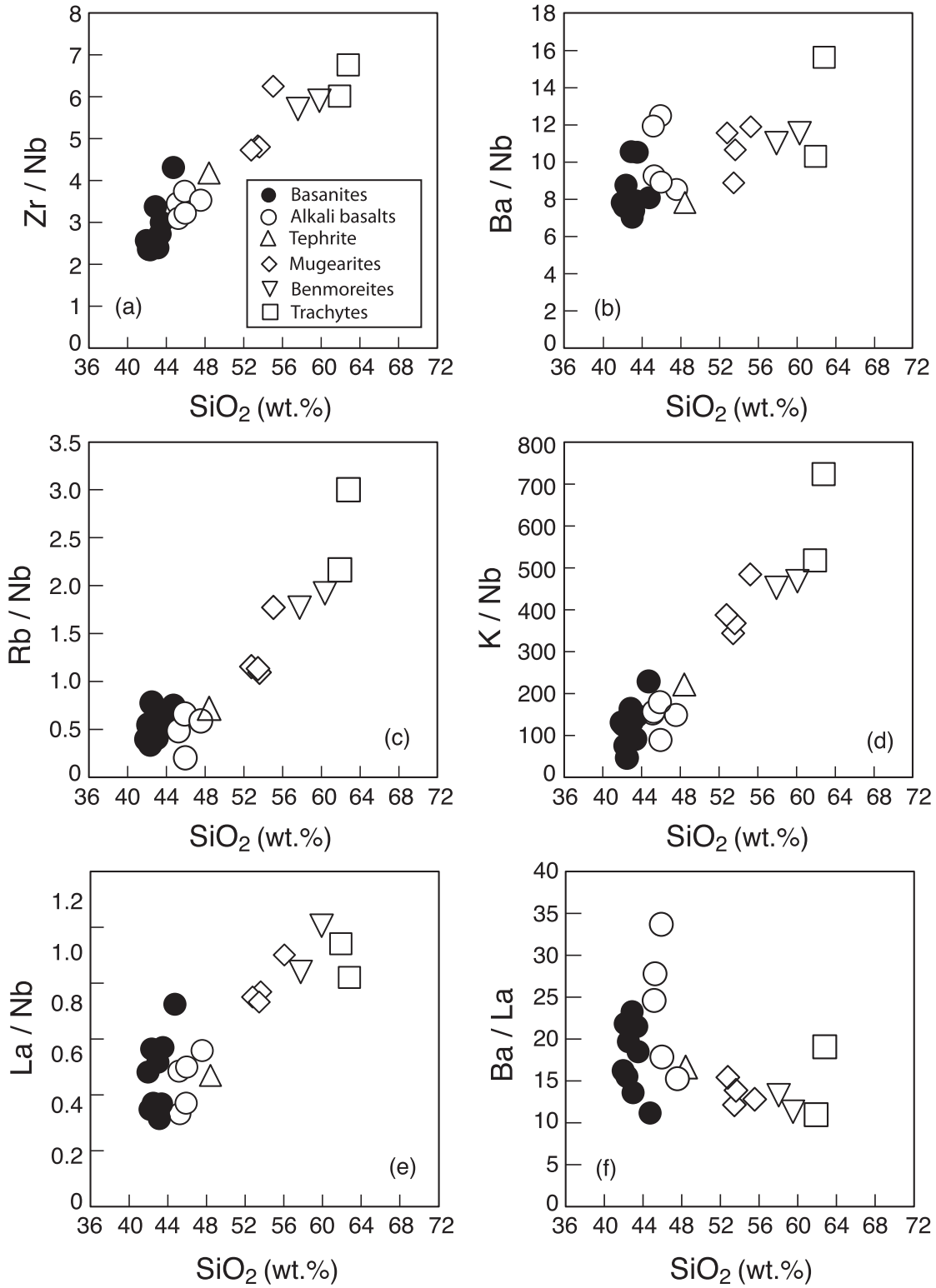

Fig. 5. (a) Zr/Nb vs SiO_2, (b) Ba/Nb vs SiO_2, (c) Rb/Nb vs SiO_2, (d) K/Nb vs SiO_2, (e) La/Nb vs SiO_2 and (f) Ba/La vs SiO_2 for the Siebengebirge lavas.

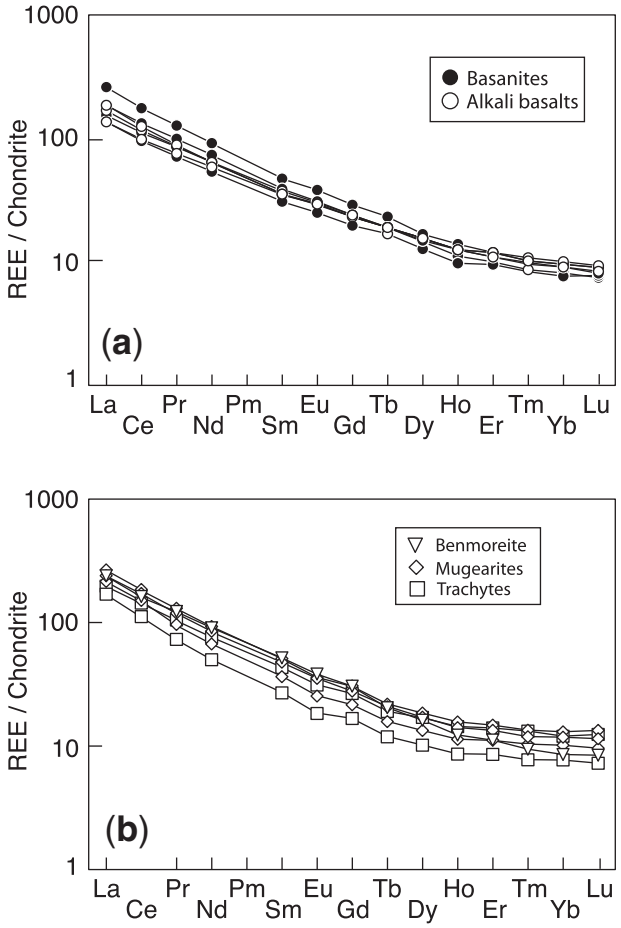

Fig. 6. Chondrite-normalized REE patterns of (a) basanites and alkali basalts and (b) differentiated rocks from the Siebengebirge area. Normalization values from Boynton (1984).

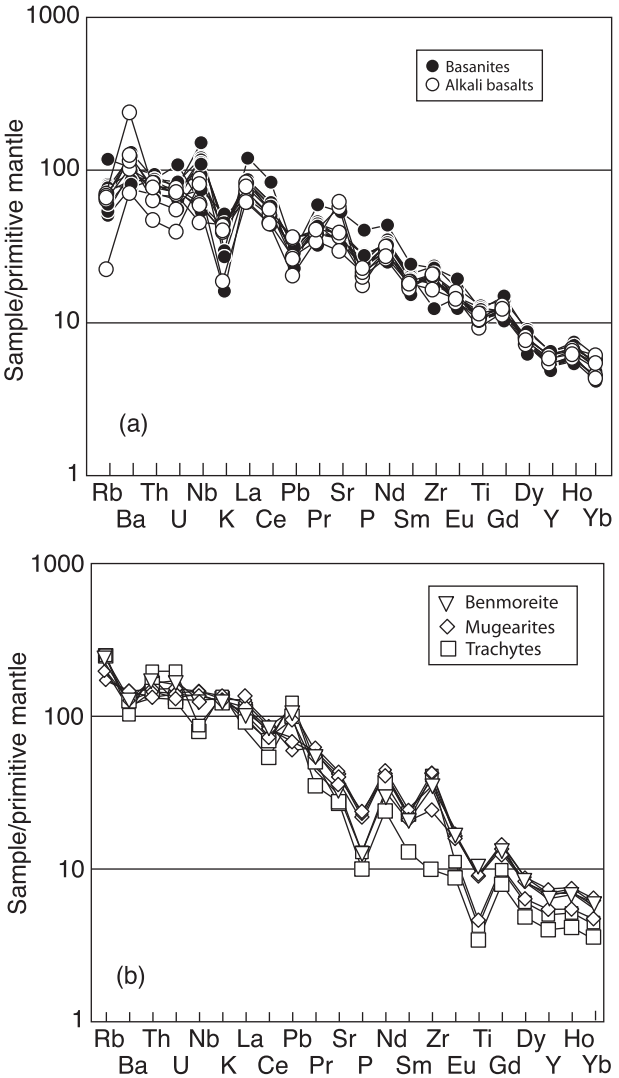

Fig. 7. Primitive mantle-normalized incompatible element patterns of (a) basanites and alkali basalts and (b) differentiated rocks from the Siebengebirge area. Normalization values from Sun & McDonough (1989).

Sr–Nd–Pb-O isotope compositions

Sr–Nd–Pb-O isotope data are reported in Table 3 and in Table 3 of the Supplementary Data in the Electronic Appendix. The samples plot in the depleted field relative to Bulk Earth in the Sr–Nd isotope diagram (Fig. 9). Initial Sr and Nd isotope data for the primitive basanites and alkali basalts form an elongated trend from more depleted compositions close to that of the European Asthenospheric Reservoir (EAR; Cebriá & Wilson, 1995) towards Bulk Earth values. Generally, this trend is broadly similar to the trends defined by Cenozoic mafic alkaline rocks from elsewhere in Germany (Wörner *et al.*, 1986; Wedepohl *et al.*, 1994; Hegner *et al.*, 1995; Jung & Masberg, 1998; Jung & Hoernes, 2000; Bogaard & Wörner, 2003; Haase *et al.*, 2004; Jung *et al.*, 2006) and also to other CEVP provinces, such as the French Massif Central, Poland, Eger Graben and the Pannonian basin (Downes, 1984; Alibert *et al.*, 1987; Blusztajn & Hart, 1989; Wilson & Downes, 1991, 2006; Embey-Isztin *et al.*, 1993; Harangi, 1994; Downes *et al.*, 1995; Haase & Renno, 2008). It is noteworthy that the trend defined by the Siebengebirge lavas is similar to that of the neighbouring Tertiary Eifel and Westerwald volcanic fields (Wörner *et al.*, 1986; Haase *et al.*, 2004; Jung *et al.*, 2006). The more differentiated samples have more radiogenic $^{87}Sr/^{86}Sr$ and less radiogenic $^{143}Nd/^{144}Nd$ than the mafic alkaline lavas and some of them overlap with the compositional fields of Eifel lower crustal granulite xenoliths (Fig. 9).

The Pb isotope compositions of the basanites and alkali basalts overlap and are variable, defining a sample population close to the Northern Hemisphere Reference Line (NHRL). This trend ranges from high $^{206}Pb/^{204}Pb$ ratios (19·8) similar to the EAR (Wilson & Downes, 2006) to more unradiogenic values (19·0) similar to other volcanic

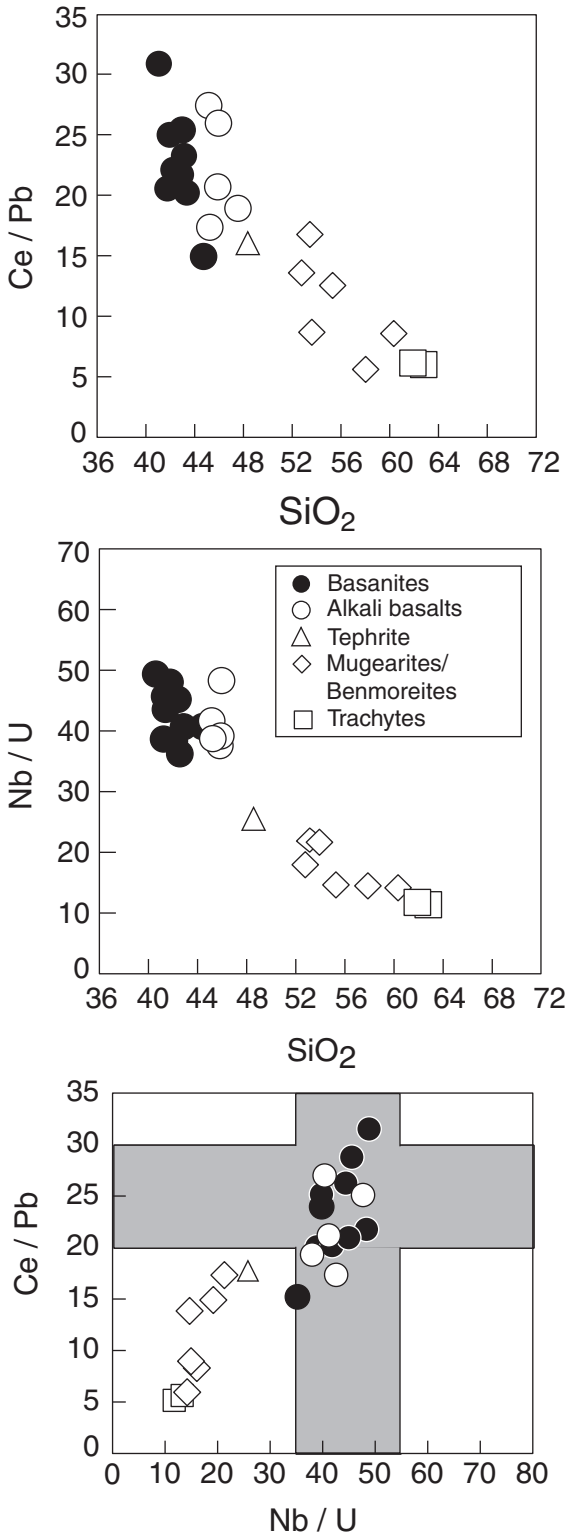

Fig. 8. (a) Ce/Pb vs SiO_2, (b) Nb/U vs SiO_2 and (c) Nb/U vs Ce/Pb covariation for the Siebengebirge mafic alkaline lavas and more differentiated rocks. The grey bars in (c) denote the range of Ce/Pb and Nb/U in oceanic basalts (Hofmann *et al.*, 1986).

provinces from the CEVP (Fig. 10). The differentiated lavas have slightly lower $^{206}Pb/^{204}Pb$ ratios but higher $^{207}Pb/^{204}Pb$ ratios than most of the mafic lavas.

The oxygen isotope compositions of the mafic lavas are highly variable and range from 5·9 to 8·0‰ (Supplementary Data, Electronic Appendix Table 3). The more evolved lavas have higher and even more variable oxygen isotope composition between 6·9 and 12·9‰. The high $\delta^{18}O$ values indicate that both mafic and felsic lavas were affected by low-temperature hydrous alteration. When corrected for late-stage alteration according to the procedure given by Ferrara *et al.* (1985), the primitive basalts have $\delta^{18}O$ values between 5·7 and 7·4‰ and in the more differentiated lavas the $\delta^{18}O$ values range from 6·3 to 10·3‰. Whether or not the correction procedure outlined by Ferrara *et al.* (1985) gives the correct magmatic $\delta^{18}O$ value is a matter of debate. One way to test this is to plot the corrected $\delta^{18}O$ whole-rock values against the $\delta^{18}O$ values obtained on minerals from the same sample. This is shown in Fig. 4 of the Supplementary Data (Electronic Appendix), where the $\delta^{18}O$ values of constituent minerals are shown. The very good correlation between corrected $\delta^{18}O$ whole-rock values and $\delta^{18}O$ values obtained on mineral separates indicates that the correction procedure works in this case and that the whole-rock values where no mineral data are available can be used for petrogenetic considerations. The low $\delta^{18}O$ values of the basanites and alkali basalts are similar to the average of 6·1 ±0·5‰ obtained for some basalts from the Rhine graben (Harmon & Hoefs, 1995) and also to the average of continental intraplate basalts (6·1 ±0·7‰; Harmon & Hoefs, 1995). It is noteworthy that there is an apparent positive correlation between $\delta^{18}O$ values and $^{87}Sr/^{86}Sr$ ratios and SiO_2 for all lavas (Supplementary Data, Electronic Appendix Fig. 4). Bearing this in mind, approximately half of the $\delta^{18}O$ values may represent near-primary values, which, in the case of the primitive lavas, may reflect a heterogeneous mantle source with respect to the oxygen isotope composition. For the differentiated lavas, processes other than partial melting and fractional crystallization [i.e. assimilation–fractional crystallization (AFC) processes] may be responsible for some of the higher $\delta^{18}O$ values. Values above *c.* 10‰ may have resulted from hydrous low-temperature alteration processes.

DISCUSSION

Fractional crystallization

Most of the basanites and alkali basalts from the Siebengebirge volcanic field have MgO and Ni contents high enough for these rocks to represent near-primary magmas (MgO > 10 wt %, Ni > 200 ppm; e.g. Hart & Davis, 1978). Samples with higher Ni (>300 ppm) and Cr (>500 ppm) abundances are probably affected by accumulation of xenocrystic olivine and clinopyroxene. Some of

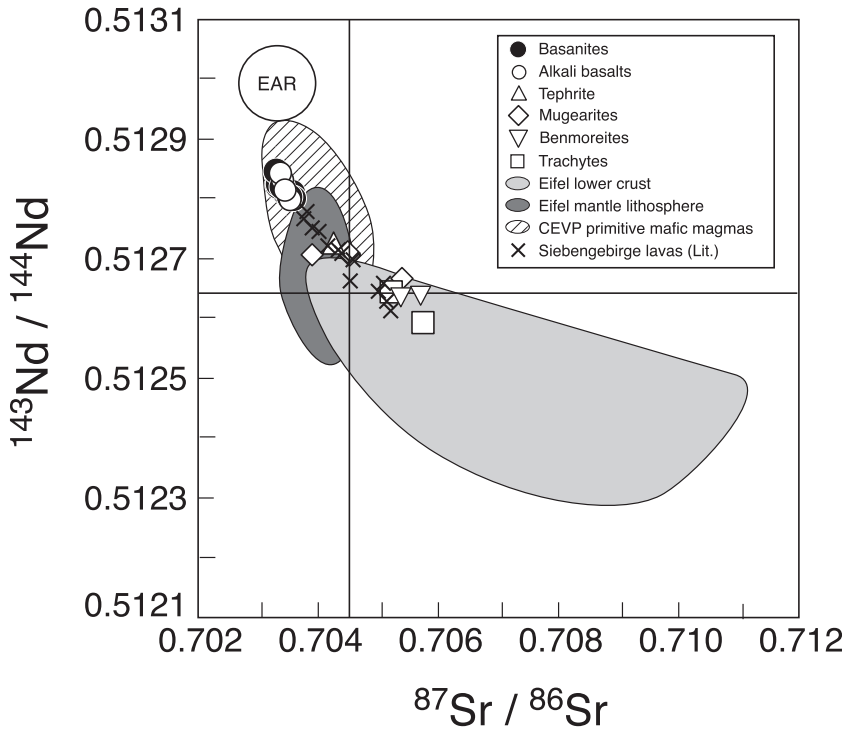

Fig. 9. $^{143}Nd/^{144}Nd$ vs $^{87}Sr/^{86}Sr$ diagram showing the data for the Siebengebirge mafic alkaline lavas and more differentiated rocks. Dark grey area represents peridotite xenolith data representative of the lithospheric mantle beneath the nearby Eifel volcanic field from Stosch & Lugmair (1986) and Witt-Eickschen *et al.* (1998, 2003). Light grey field represents lower crustal xenolith data from the nearby Eifel volcanic field (Stosch & Lugmair, 1984; Loock *et al.*, 1990). EAR denotes the European Asthenospheric Reservoir (Cebriá & Wilson, 1995). Literature data for Siebengebirge volcanic rocks are from Wedepohl *et al.* (1994).

the basanites and alkali basalts have lower concentrations of MgO, Ni and Cr and for these samples fractionation of olivine and clinopyroxene is likely. Similarly, decreasing CaO and increasing Al_2O_3 leads to decreasing CaO/Al_2O_3 ratios with increasing SiO_2, which is also consistent with clinopyroxene fractionation.

The differentiated lavas have lower concentrations of MgO, Ni and Cr, consistent with olivine and clinopyroxene fractionation. Constant Al_2O_3 contents and the lack of negative Eu anomalies indicate that plagioclase was not a major fractionating mineral phase at this stage. Some basanites and alkali basalts contain green-core clinopyroxenes; in accordance with previous studies (e.g. Duda & Schmincke, 1985; Jung & Hoernes, 2000; Haase *et al.*, 2004) the appearance of green-core clinopyroxenes is evidence for high-pressure or, at least, polybaric fractionation of the host magma. This conclusion is compatible with the work of Sachs & Hansteen (2000), who showed that comparable alkaline magmas stagnated in the lower crust at pressures of about 0·65 GPa, equivalent to 20 km depth. One fractionated sample (Supplementary Data, Electronic Appendix Fig. 3) shows a deficiency of the MREE relative to the LREE and HREE, which can be explained by significant fractionation of amphibole and/or titanite. In accordance with previous studies on the evolution of the European alkaline magma series (Downes, 1984; Wilson *et al.*, 1995a), it is suggested that the alkali basalts represent the parental magmas from which the more differentiated rocks originated by fractional crystallization.

Crustal contamination

Major element and compatible trace element variations in the basanites, alkali basalts and the more differentiated rocks of the Siebengebirge indicate that fractional crystallization processes affected the magmas during ascent. However, some trace element data correlate with isotope composition, indicating that crustal contamination was a likely process affecting the alkaline lavas. The lower crust beneath Germany is mainly composed of mafic and felsic granulites (Mengel *et al.*, 1991; Sachs & Hansteen, 2000). Lower crustal xenoliths from the nearby Eifel area have been extensively studied (Stosch & Lugmair, 1984; Stosch *et al.*, 1986, 1992; Loock *et al.*, 1990; Rudnick & Goldstein, 1990). These granulites have Sr–Nd isotope compositions that extend from Bulk Earth values towards more unradiogenic $^{143}Nd/^{144}Nd$ and more radiogenic $^{87}Sr/^{86}Sr$ isotope compositions (Fig. 9). Felsic granulites tend to have more radiogenic $^{87}Sr/^{86}Sr$ isotope compositions, although some mafic granulites are also fairly radiogenic in $^{87}Sr/^{86}Sr$. The basanites and alkali basalts have higher $^{143}Nd/^{144}Nd$

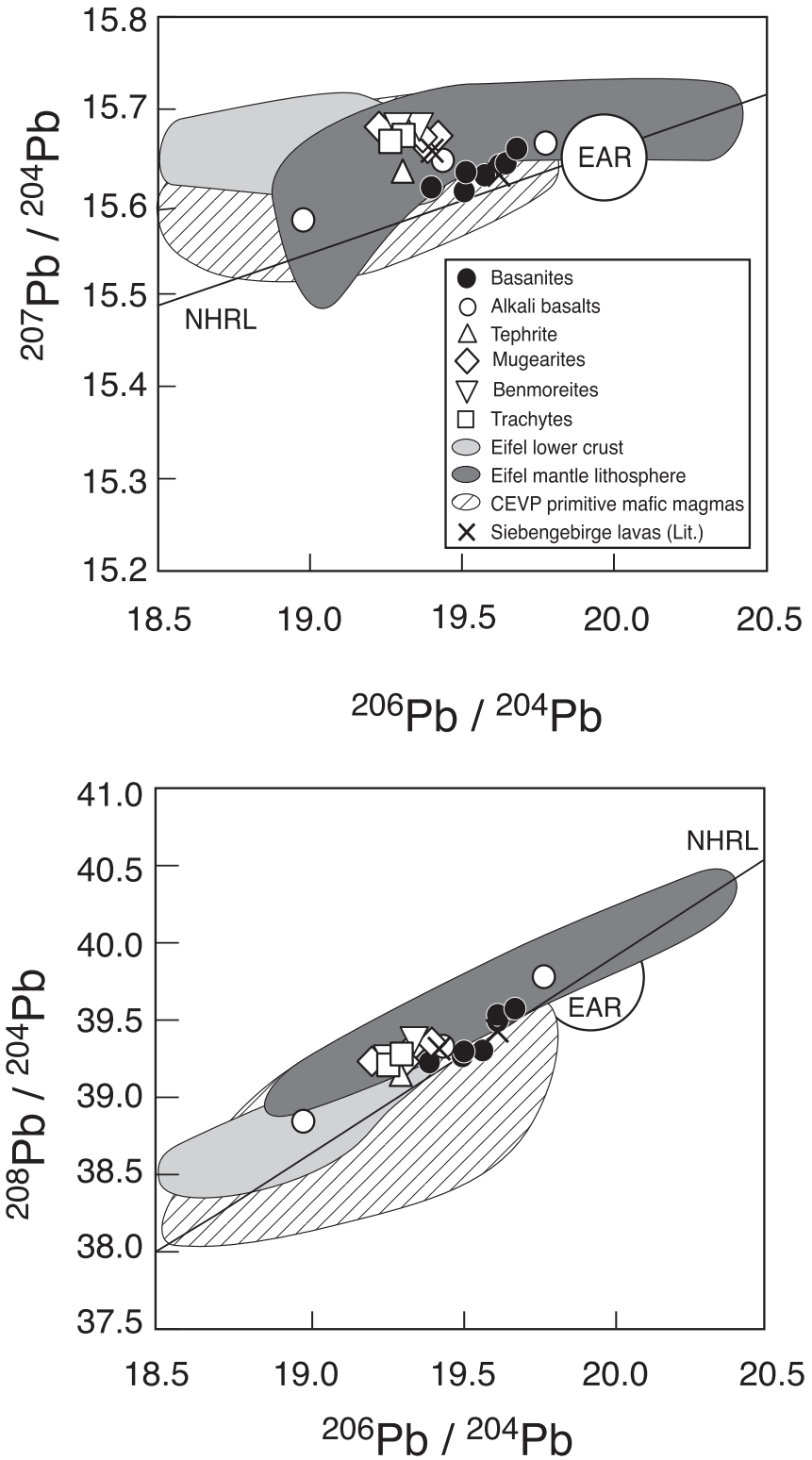

Fig. 10. Plot of (a) $^{207}Pb/^{204}Pb$ and (b) $^{208}Pb/^{204}Pb$ vs $^{206}Pb/^{204}Pb$ for Siebengebirge mafic and differentiated alkaline lavas. Abbreviations and fields for mantle lithosphere, CEVP magmas and crustal xenoliths as in Fig. 9. Pb isotopes for Siebengebirge lavas from the literature are from Wedepohl & Baumann (1999). NHRL is the Northern Hemisphere Reference Line (Hart, 1984).

and lower $^{87}Sr/^{86}Sr$ than the lower crustal xenoliths, but some of the more differentiated rocks overlap with the Sr–Nd isotope composition of the xenoliths (Fig. 9). The Pb isotope compositions of the xenoliths plot above the NHRL in $^{207}Pb/^{204}Pb$ vs $^{206}Pb/^{204}Pb$ and $^{208}Pb/^{204}Pb$ vs $^{206}Pb/^{204}Pb$ diagrams (Fig. 10) and are displaced towards higher $^{207}Pb/^{204}Pb$ and $^{208}Pb/^{204}Pb$ ratios at a given $^{206}Pb/^{204}Pb$ ratio. The Pb isotope compositions of the differentiated lavas extend towards high $^{207}Pb/^{204}Pb$ ratios up to 15·68. Such high $^{207}Pb/^{204}Pb$ ratios indicate assimilation of an ancient crustal component having a high U/Pb ratio. Similarly, the $^{87}Sr/^{86}Sr$–SiO_2–$\delta^{18}O$ relationships (Supplementary Data, Electronic Appendix Fig. 4) indicate that crustal contamination also played an important role here. The range in $\delta^{18}O$ of the differentiated rocks (6–11‰) is probably too large to be related to crustal contamination alone and low-temperature modification may have played a role here also but the correlation with $^{87}Sr/^{86}Sr$ also points to crustal contamination. However, the high $\delta^{18}O$ values of the trachytes and latites may lead to an overestimate of crustal contamination owing to possible low-temperature modification of the primary values.

It is commonly assumed that assimilation of lower crustal rocks and fractional crystallization would have occurred simultaneously. However, thermal considerations suggest that bulk assimilation of lower crustal rocks is unlikely and that contamination of the fractionating alkali basaltic magma with a partial melt of the lower crustal wall-rocks is more appropriate. The heat required for partial melting is released by the fractional crystallization process. Recent models have explained this process in terms of energy-constrained assimilation–fractional crystallization (EC-AFC; Spera & Bohrson, 2001). This model was used to test the influence of concurrent crustal assimilation and fractional crystallization upon the composition of the differentiated lavas from the Siebengebirge using the parameters given in Table 4. In contrast to the model parameters given by Spera & Bohrson (2001), we used a slightly higher initial temperature for the lower crust of 850°C. This higher temperature is in agreement with recent estimates of lower crustal temperatures from the nearby Eifel province (>800°C, Sachs & Hansteen, 2000), and probably mirrors more closely the effects of rifting, uplift of the asthenosphere–lithosphere boundary and continuing magmatism in Tertiary–Quaternary times. Moreover, at this high inferred temperature, high rates of assimilation relative to fractional crystallization are likely (Reiners *et al.*, 1995).

In our model, we used sample SG 3 to represent the parental melt; this is an unfractionated basanite with high MgO (11·5 wt %), high Cr and Ni abundances (337 and 270 ppm, respectively) and unradiogenic $^{87}Sr/^{86}Sr$ and radiogenic $^{143}Nd/^{144}Nd$ isotope ratios (Tables 2 and 3). As the assimilant we used sample S 32 (Stosch & Lugmair, 1984; Loock *et al.*, 1990), which is a granulite xenolith with fairly high $^{87}Sr/^{86}Sr$ and low $^{143}Nd/^{144}Nd$ (Table 4). It can be seen that the range in Sr, Nd and Pb isotope composition of the differentiated lavas can be reproduced by an EC-AFC model (Fig. 11), implying that EC-AFC processes played an important role in the evolution of the differentiated lavas from the Siebengebirge. A similar relationship can be demonstrated using $^{207}Pb/^{204}Pb$ isotope systematics (not shown in detail here). Based on this model, the isotope composition of the differentiated lavas can be explained by 40–50% fractional crystallization combined with 10–30% assimilation of a granulite-facies lower crust with an isotope composition similar to that of S 32. The degrees of assimilation are rather high and probably unrealistic; however, the composition of the lower crust beneath the Rhenish Massif is highly variable with respect to its isotope composition and more suitable endmembers may exist.

Some trace element constraints are also compatible with assimilation of crustal material. Crustal rocks in general and the lower crustal xenoliths from the Rhenish Shield in particular have Ce/Pb ratios <20 and Nb/U ratios between *c.* 10 and 50 (Haase *et al.*, 2004). In contrast, oceanic basalts have high Ce/Pb (25 ± 5) and Nb/U ratios (47 ± 10) that are commonly not fractionated during

Table 4: Compositions and parameters used for the EC-AFC model calculations (Spera & Bohrson, 2001)

Magma liquidus temperature	1350°C		
Magma temperature t_{m0}	1350°C		
Assimilant liquidus temperature	1100°C		
Country rock temperature t_{a0}	850°C		
Solidus temperature t_s	950°C		
Magma specific heat capacity C_{pm}	1484 J kg^{-1} K		
Assimilant specific heat capacity C_{pa}	1388 J kg^{-1} K^{-1}		
Crystallization enthalpy	396000 J kg^{-1}		
Fusion enthalpy	354000 J kg^{-1}		
Equilibration temperature	980°C		
Element (in ppm):	Sr	Nd	Pb
Melt SG 3	708	37·3	7·44
Bulk D_o	0·1	0·1	0·1
Enthalpy	0	0	0
Assimilant S 32	1325	36·9	4·57
Bulk D_o	0·5	0·25	0·1
enthalpy	0	0	0
	$^{87}Sr/^{86}Sr$	$^{143}Nd/^{144}Nd$	$^{206}Pb/^{204}Pb$
Melt SG 3	0·703549	0·512813	19·56
Assimilant S 32	0·709480	0·512198	19·04

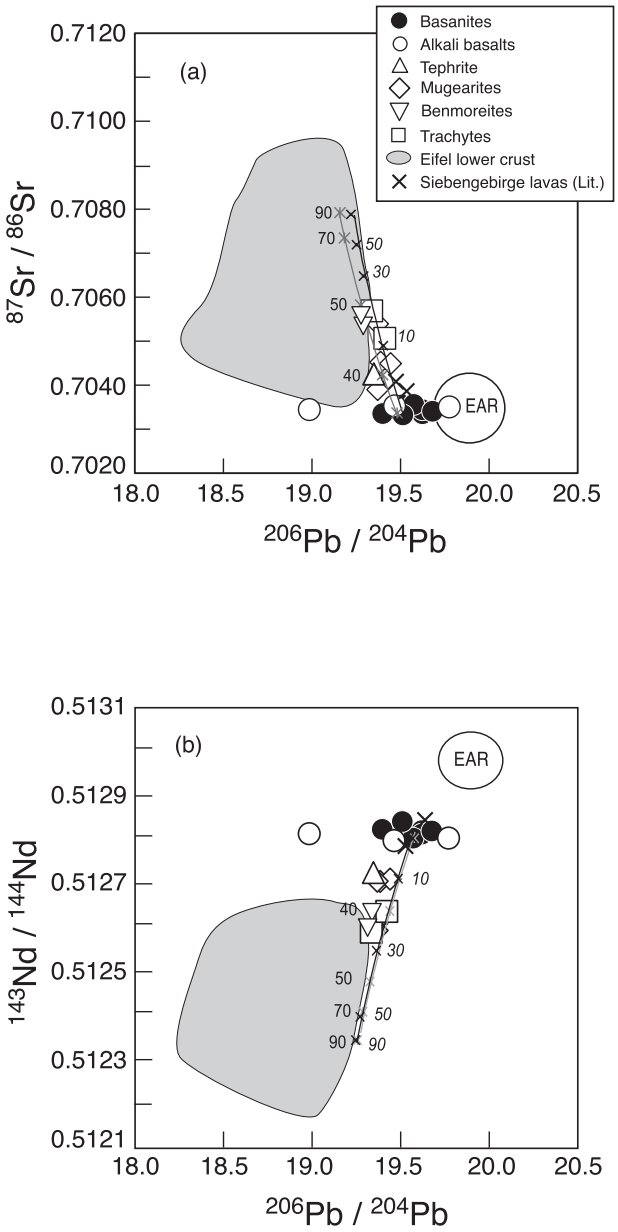

Fig. 11. (a) $^{87}Sr/^{86}Sr$ vs $^{206}Pb/^{204}Pb$ and (b) $^{143}Nd/^{144}Nd$ vs $^{206}Pb/^{204}Pb$ for mafic and differentiated alkaline lavas from the Siebengebirge. Lines show the results of EC-AFC calculations with model parameters and endmember compositions from Table 4. Grey lines with regular-font numbers denote mass crystallized and black lines with italic numbers denote mass assimilated (both as wt %).

mantle melting and therefore reflect the composition of the Earth's mantle (Hofmann *et al.*, 1986). Most basanites from the Siebengebirge have Ce/Pb ratios between 20 and 32. These samples have Nb/U ratios between 35 and 50. Other mafic lavas have lower Ce/Pb ratios between 14 and 19 with Nb/U ranging from 35 to 40. The composition of these mafic lavas, as well as the composition of the differentiated lavas with low Ce/Pb and low Nb/U, extends towards some lower crustal xenoliths with low Ce/Pb ratios and low Nb/U ratios (Sachs & Hansteen, 2000; Fig. 8).

Magma generation in the Siebengebirge volcanic field

It is generally accepted that the upper mantle is composed predominantly of peridotite with minor amounts of pyroxenite, both with or without garnet. Primitive alkaline, silica-undersaturated magmas such as basanites can form at high pressure from garnet peridotite sources (Kushiro, 1996), but usually not from garnet pyroxenite [Rapp *et al.*, 1991; however, for a different view see Hirschmann *et al.* (2003) and Kogiso *et al.* (2003)]. There is considerable geochemical (e.g. Hofmann, 1997) and geophysical (e.g. van der Hilst *et al.*, 1997) evidence that the upper mantle is heterogeneous and this heterogeneity may result from recycling of oceanic lithosphere at subduction zones. Moreover, evidence from experimental studies (e.g. Spandler *et al.*, 2008) and studies of melt inclusions (Sobolev *et al.*, 2005, 2007) also indicate that recycled oceanic crust, now preserved as pyroxenite or eclogite, may be important constituents of the upper mantle. On the other hand, other studies (e.g. Niu & O'Hara, 2003) indicate that direct melting of SiO_2-saturated pyroxenite sources is improbable, given the SiO_2-undersaturated nature of most OIBs, which are also characterized by high MgO, Ni and Cr abundances and LREE enrichment. Early experimental evidence (e.g. Yaxley & Green, 1998) suggested that direct melting of pyroxenite or eclogite at pressures >2·5 GPa produces andesitic liquids but not alkaline melts, but more recent experiments have yielded alkali basaltic melts at pressures up to 2·5 GPa (Keshav *et al.*, 2004). Migration of SiO_2-rich andesitic melts into peridotite will yield a heterogeneous, refertilized peridotite with a different opx:cpx:ol ratio, which upon melting can produce strongly ne-normative mafic melts. Ne-normative nephelinites and basanites can also be generated by partial melting of amphibole- and/or phlogopite-bearing garnet or spinel peridotite at pressures >2 GPa and temperatures >1360°C in the presence of CO_2 (Mysen & Kushiro, 1977; Hirose, 1997) or at much lower temperatures of 1200–1250°C and pressures of 2·8–3·0 GPa (Mengel & Green, 1986; Thibault *et al.*, 1992). In addition, partial melting of amphibole-rich sources may produce ne-normative alkaline melts (Pilet *et al.*, 2008). Generally, the formation of Si-undersaturated melts requires the presence of H_2O and CO_2 (Brey & Green, 1977; Mengel & Green, 1986; Thibault *et al.*, 1992; Hirose, 1997).

Melting of spinel- or garnet-peridotite upper mantle sources can be illustrated and modelled using REE systematics; for example, variation of La/Yb vs Dy/Yb (Fig. 12; Thirlwall *et al.*, 1994; Baker *et al.*, 1997). Assuming the presence of residual garnet and relatively small degrees of melting, such plots can easily distinguish between melting in

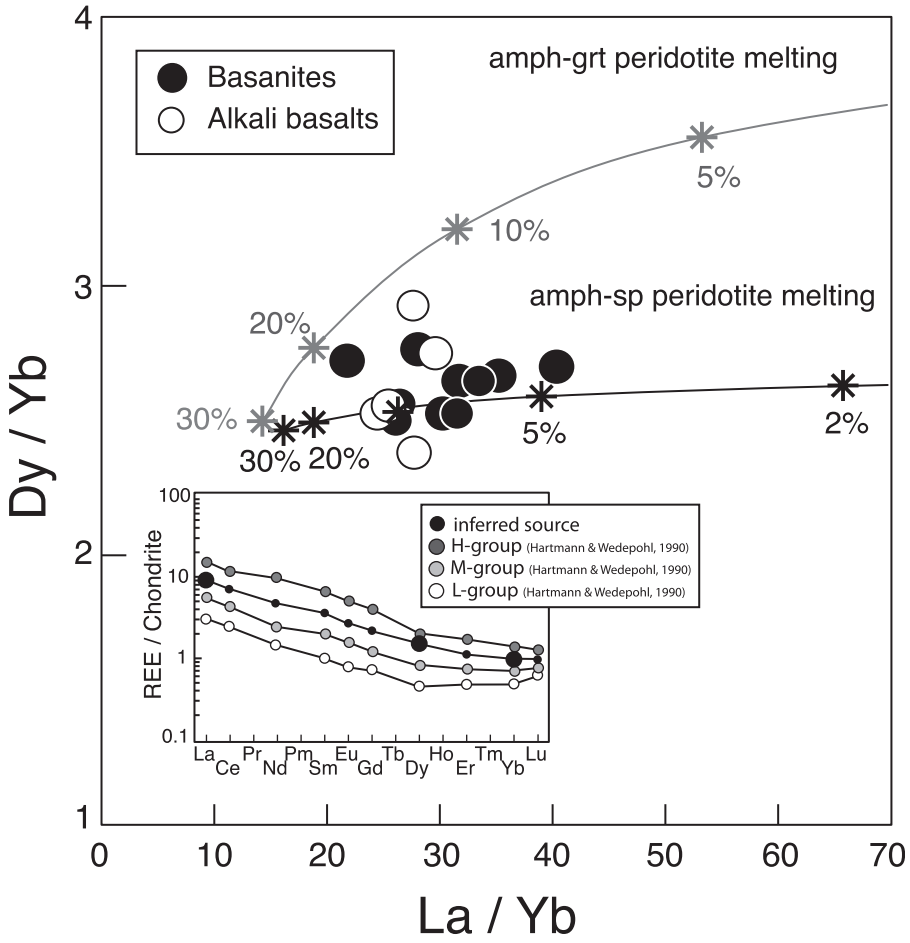

Fig. 12. Dy/Yb vs La/Yb for the Siebengebirge basalts. Partial melting curves were calculated using a non-modal, batch melting model (Shaw, 1970). Sources are amph–grt-peridotite (cpx 0·20, opx 0·15, ol 0·58, grt 0·02, amph 0·05) that melts in the proportions cpx 0·40, opx 0·20, ol 0·10, grt 0·10, amph 0·20, and amph–sp-peridotite (cpx 0·20, opx 0·15, ol 0·58, sp 0·02, amph 0·05) that melts in the proportions cpx 0·40, opx 0·20, ol 0·10, sp 0·10, amph 0·20. Adjusted source composition (La 2·7 ppm, Yb 0·19 ppm, Dy 0·45 ppm) is within the range of 36 peridotite xenoliths from the Hessian Depression (Hartmann & Wedepohl, 1990; see inset). Mineral–melt distribution coefficients were taken from McKenzie & O'Nions (1991), Hart & Dunn (1993), Kelemen *et al.* (1993), Johnson (1998) and LaTourette *et al.* (1995). Numbers on model curves indicate the per cent melting.

the garnet peridotite stability field and in the spinel peridotite stability field because of the strong fractionation of HREE by garnet. Additionally, mixing of melts from distinct sources should produce linear arrays in such a diagram. Most of the basanites and alkali basalts from the Siebengebirge appear to form a coherent group (Fig. 12). The data indicate that, in contrast to studies of other Cenozoic volcanic districts of Germany (Westerwald: Haase *et al.*, 2004; Tertiary Hocheifel: Jung *et al.*, 2006) the samples do not plot on mixing lines between melts from garnet peridotite and melts from spinel peridotite. Instead, most samples seem to originate by partial melting of a spinel- and amphibole-bearing peridotite source. The basanites and alkali basalts display a negative correlation between K/La and Ce/Yb_N (Fig. 13), implying that partial melting of a simple four-phase peridotite is not likely because low-melt fractions from such a source have both high Ce/Yb_N and K/La ratios (Haase *et al.*, 2004). It is, therefore, possible that a residual mineral phase that fractionates K from La was present during partial melting. This mineral phase is more likely to be amphibole rather than phlogopite, because phlogopite fractionates K/La even more efficiently than amphibole and also fractionates Ba from La. Ba concentrations are high in the primitive Siebengebirge lavas, which argues against significant amounts of phlogopite in the solid residue. There is also a negative correlation between Ce/Pb and K/La and a positive correlation between Ce/Pb and Ce/Yb_N. Decreasing Ce/Pb ratios are accompanied by decreasing Ce/Yb_N ratios, suggesting that the variation of Ce/Pb is, at least partially, controlled by variable degrees of melting. Fractionation of olivine and clinopyroxene will not cause

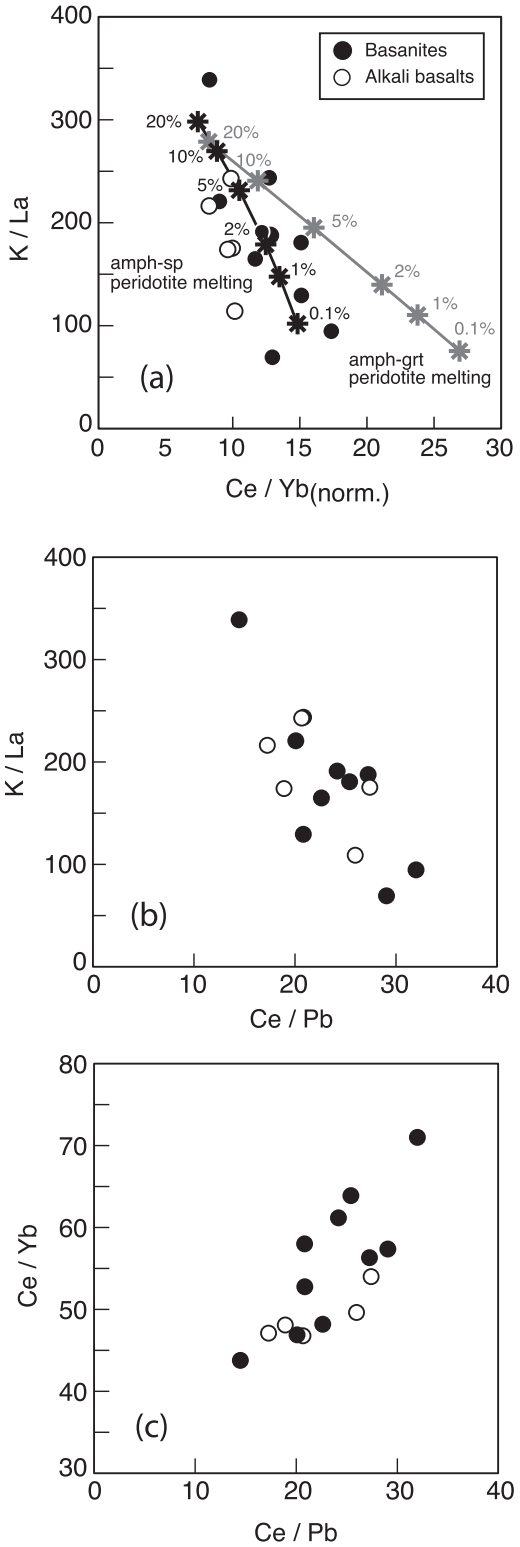

Fig. 13. (a) Variation of K/La vs chondrite-normalized Ce/Yb for mafic alkaline lavas from the Siebengebirge. Partial melting curves were calculated using a non-modal, batch melting model (Shaw, 1970) with the sources and melting modes given in Fig. 13. The source composition has 800 ppm K, 2·7 ppm La, 4·5 ppm Ce and 0·19 ppm Yb, which is within the range of 36 peridotite xenoliths from the Hessian Depression (Hartmann & Wedepohl, 1990). Mineral–melt distribution coefficients are from McKenzie & O'Nions (1991), Hart & Dunn (1993), Kelemen *et al.* (1993), Johnson (1998) and LaTourette *et al.* (1995). It should be noted that a negative correlation between K/La and $Ce/Yb_{(norm.)}$ is possible only when peridotite sources carrying hydrous mineral phases (amphibole, phlogopite) are considered. (b) Variation of K/La vs Ce/Pb and (c) Ce/Yb vs Ce/Pb. Samples with high K/La and low $Ce/Yb_{(norm.)}$ are probably influenced by crustal contamination, as these samples have low Ce/Pb ratios. Correlation of Ce/Pb with K/La and Ce/Yb indicate variable degrees of partial melting of a peridotite source containing residual K-bearing mineral phases with a contribution from variable amounts of spinel and garnet. Only a few samples with Ce/Pb < 20 appear to be influenced by crustal contamination.

significant variation of Ce/Pb; however, Ce/Pb ratios are also negatively correlated with K/La ratios. This suggests that some of the variation in Ce/Pb (in samples with Ce/Pb > 20) is controlled by residual K-bearing mineral phases. This suggestion is also supported by the data of Rosenbaum (1993), who showed that amphibole and phlogopite are important hosts for Pb in the mantle. In conclusion, the mantle source of the Siebengebirge lavas probably contains amphibole, which is compatible with petrographic observations from lithospheric mantle xenolith studies from elsewhere in the CEVP (Witt-Eickschen & Kramm, 1998; Witt-Eickschen *et al.*, 1998, 2003).

Previous geophysical data (e.g. Babuska & Plomerová, 1988, 1992) indicated that the lithosphere–asthenosphere boundary beneath the Rhenish shield is located at ~60 km depth. However, more recent estimates (Babuska & Plomerová, 2006) suggest that the lithosphere–asthenosphere boundary beneath the Rhenish shield is probably deeper, probably at ~90–100 km depth. Geochemical arguments have been used to infer that amphibole is not stable in the convective upper mantle or mantle plumes and must therefore be restricted to the lithospheric mantle (Class & Goldstein, 1997). If it is accepted that amphibole is present in the mantle source of the Siebengebirge lavas this would restrict the maximum melting depth to ~90–100 km depth, in accordance with the stability of pargasite down to ~90 km depth (Green *et al.*, 2010). Moreover, the REE modelling and negative Rb and K anomalies in mantle-normalized trace element diagrams presented here are compatible with the presence of amphibole and therefore seem to indicate a lower lithospheric contribution to these basalts. The transition from garnet to spinel peridotite is estimated to occur at 2·5–3·0 GPa equivalent to 75–90 km depth (McKenzie & Bickle, 1988; Robinson & Wood, 1998). Because the basanites and alkali basalts formed in the stability field of spinel peridotite in the presence of amphibole, it is suggested that the melting region is located at less than 2·5 GPa and ~1150°C if the stability field of pargasite according to Green *et al.* (2010) is considered (Fig. 14). Amphibole may have formed by

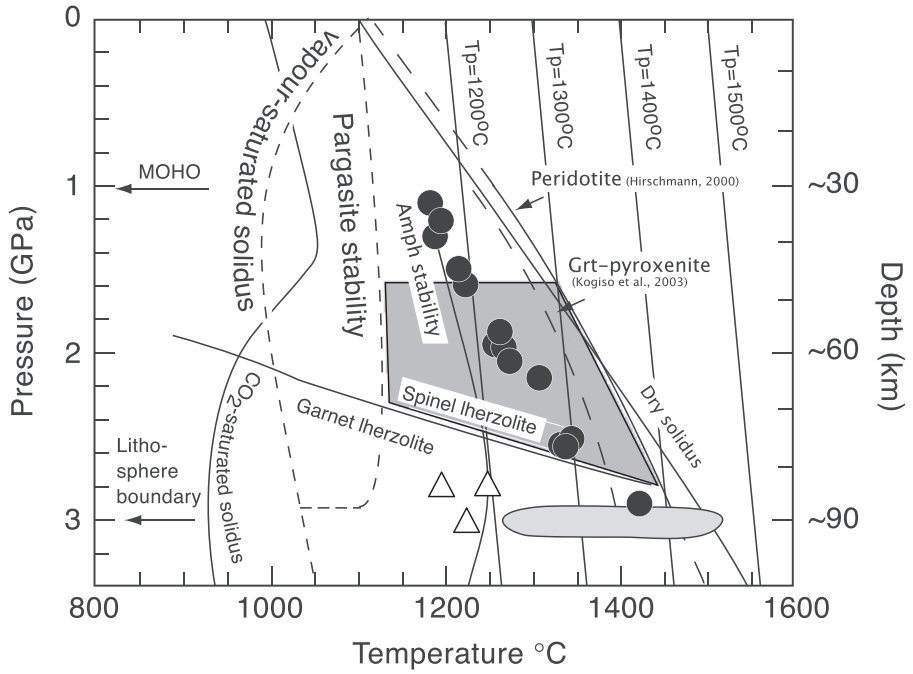

Fig. 14. Pressure–temperature diagram to illustrate the potential source region of the mafic alkaline magmas from the Siebengebirge. Solidi for dry mantle and CO_2-saturated mantle are from McKenzie & Bickle (1988) and Falloon & Green (1990), respectively. Vapour-saturated solidus and the stability curve for pargasite are from Green *et al.* (2010). Also shown are adiabats for various mantle potential temperatures. Stability fields for spinel and garnet peridotite and amphibole in upper mantle rocks are from Falloon & Green (1990), Foley (1991) and Robinson & Wood (1998). Solidus for peridotite after Hirschmann (2000) and solidus for garnet pyroxenite after Kogiso *et al.* (2003). Crustal thickness (Moho) is adopted from Prodehl *et al.* (1992) and the lithosphere–asthenosphere boundary is from Babuska & Plomerova (2006). Open triangles mark the experimental results of phlogopite–garnet peridotite melting from Mengel & Green (1986) and Thibault *et al.* (1992). The light grey area denotes the area where partial melting gives rise to melts similar to primitive alkali olivine basalts (Dasgupta *et al.*, 2007) whereas the dark grey area approximates the P–T conditions for the generation of the basanites from the Siebengebirge. Black circles represent inferred P–T conditions of primary melts from the Siebengebirge using the algorithm of Lee *et al.* (2009). It should be noted that, based on geochemical arguments discussed in the text (presence of restitic amphibole, predominance of melts from spinel peridotite), these temperature and pressure estimates must be viewed as maximum estimates.

metasomatism owing to migration of small-degree melts from an upwelling plume beneath the Rhenish Massif. This conclusion is also compatible with the view that partial melting in the upper mantle beneath Europe very probably requires a volatile-rich mantle source (Wilson & Downes, 2006), which may be represented by the inferred amphibole-bearing peridotite source of the mafic Siebengebirge lavas. Recently, Dasgupta *et al.* (2007) have argued that partial melting of volatile-rich (carbonated) peridotite can yield alkaline melts with major element characteristics (43–45 wt % SiO_2; 9–12 wt % Al_2O_3; 12–16 wt % CaO; 1–2 wt % TiO_2; 10–11 wt % FeO; 2–3 wt % Na_2O) similar to most alkaline OIB. Such melts also show some similarities to continental alkaline volcanic rocks in general and to the primitive basanites from the Siebengebirge in particular (42–45 wt % SiO_2; 11–13 wt % Al_2O_3; 10–12 wt % CaO; 2–3 wt % TiO_2; 10–12 wt % FeO; 2–4 wt % Na_2O). According to Dasgupta *et al.* (2007), partial melting of carbonated peridotite starts at slightly higher pressures and temperatures (3 GPa; 1350–1450°C) than partial melting of amphibole-bearing spinel peridotite.

To further constrain the melting conditions of the Siebengebirge lavas, we have applied the new geothermobarometric calculations for basaltic magmas provided by Lee *et al.* (2009). Before the data can be used, several important points have to be considered. As stated by Lee *et al.* (2009), the barometer is valid only for primary mantle-derived magmas that were multiply saturated in olivine and orthopyroxene in their source regions. If the primary magma source does not have olivine and orthopyroxene, any P–T estimates will be meaningless. Although the upper mantle is believed to be largely peridotitic and hence contain both of these phases, there is growing evidence that some basaltic magmas might include a component derived from olivine-free sources, such as pyroxenites (Hirschmann *et al.*, 2003; Sobolev *et al.*, 2005). This degree of chemical heterogeneity falls outside the applicable compositional range of the thermobarometers provided by Lee *et al.* (2009). Furthermore, the barometer has not been calibrated for silica-undersaturated rocks (<40 wt % SiO_2) owing to lack of sufficient experimental data, hence it is strongly advised not to apply the barometer to magmas, such as nephelinites, leucitites,

kimberlites, etc. Whether this restriction applies to basanites with $SiO_2 > 43$, such as most basanites from the Siebengebirge, is not clear. Finally, the barometer also does not include the effects of CO_2 on silica activity; however, CO_2 is very important in the generation of silica-undersaturated magmas (Dasgupta & Hirschmann, 2006).

It is obvious from Fig. 14 that the temperature and pressure estimates using the Lee *et al.* (2009) thermobarometers seem to fit perfectly with the available experimental and geophysical data. The P–T estimates are also compatible with the generation of the lavas from predominatly spinel peridotite sources and the inferred presence of amphibole, at least in the lower pressure lavas. One important observation is that the data for the Siebengebirge lavas approach or intersect the peridotite solidus (Hirschmann, 2000) or garnet pyroxenite solidus (Kogiso *et al.*, 2003) at temperatures consistent with a mantle potential temperature of ~1400°C. There is geophysical (Ritter *et al.*, 2001) and geochemical evidence (Haase *et al.*, 2004) for a deep-seated 'hot finger' underneath the Rhenish Massif and these inferred temperatures are probably realistic. Other possibilities to produce elevated mantle temperatures include insulating effects of thick continental lithosphere that builds up heat beneath continents (Lenardic *et al.*, 2005) or that the base of the continental lithosphere becomes anomalously hot by radioactive heating associated with a zone of highly metasomatized mantle.

Mantle source of the Siebengebirge lavas

The Cenozoic volcanic rocks of Germany comprise mostly sodium-dominated alkaline rocks with the exception of some rare olivine- and quartz-tholeiites that exhibit a large range in initial $^{87}Sr/^{86}Sr$ and $^{143}Nd/^{144}Nd$. In Nd–Sr isotope space, the most mafic alkaline volcanic rocks plot between EAR (European Asthenospheric Reservoir)-like and Bulk Earth compositions. The rare quartz tholeiitic rocks are characterized by less radiogenic Nd and slightly more radiogenic Sr isotopic compositions compared with the sodic alkaline basic rocks; these have been related to magma chamber contamination at lower crustal depths via AFC processes. Lead isotopic ratios also span a relatively wide range, consistent with the involvement of DMM, HIMU and EMI-like mantle source components in the petrogenesis of the most primitive magmas (Lustrino & Wilson, 2007).

Most basanites and alkali basalts from the Siebengebirge do not appear to have been contaminated by crustal material based on their Ce/Pb vs Nb/U variation; hence, their Sr–Nd–Pb isotope compositions should reflect those of their mantle sources and, based on the large range of variation, indicate substantial isotopic heterogeneity of the mantle sources involved. The $^{87}Sr/^{86}Sr$ and $^{143}Nd/^{144}Nd$ ratios of the apparently uncontaminated Siebengebirge lavas range from 0·7033 to 0·7036 and from 0·51284 to 0·51280, respectively, which is the same as in the Eifel group (Haase *et al.*, 2004) consisting of lavas from the Eifel, Westerwald and Siebengebirge. Here, $^{87}Sr/^{86}Sr$ and $^{143}Nd/^{144}Nd$ ratios range from 0·7034 to 0·7036 and from 0·51285 to 0·51283, respectively. These features indicate that the upper mantle beneath this part of the Rhenish Massif is isotopically heterogeneous, but it is evident that all of the lavas probably had a common mantle source. On the other hand, this apparently limited range in isotopic composition may be the result of poor sampling, as the whole area (Eifel, Westerwald, Siebengebirge) was previously represented by fewer than 15 samples. In a more recent study, Jung *et al.* (2006) carried out a detailed study of the Tertiary Hocheifel area, based on 36 uncontaminated nephelinites, basanites and alkali basalts. Given that the isotope composition of these lavas is probably more representative, $^{87}Sr/^{86}Sr$ and $^{143}Nd/^{144}Nd$ range from 0·7031 to 0·7035 and from 0·51293 to 0·51274, indicating much more heterogeneity than shown by previous studies.

The $^{206}Pb/^{204}Pb$ isotope ratios display a substantial variation ranging from 19·40 to 19·78 and are, together with the data from the Tertiary Hocheifel (Jung *et al.*, 2006), the Westerwald (Haase *et al.*, 2004) and the Quaternary West Eifel (Wörner *et al.*, 1986), the highest found to date in the volcanic fields of the Rhenish Massif. One alkali basalt has a much lower $^{206}Pb/^{204}Pb$ ratio of 18·98 (Fig. 10) similar to some basanites and alkali basalts found in the Tertiary Hocheifel area, the Westerwald, the Hessian Depression and the Vogelsberg region (Wedepohl & Baumann, 1999; Bogaard & Wörner, 2003; Haase *et al.*, 2004; Jung *et al.*, 2006, 2011) representing the lower limit of $^{206}Pb/^{204}Pb$ observed in the CEVP lavas.

The composition of the shallow lithospheric mantle beneath the Rhenish Massif is relatively well known owing to numerous geochemical and isotopic investigations of spinel peridotite xenoliths from the East Eifel and West Eifel volcanic fields (Stosch & Seck, 1980; Stosch & Lugmair, 1986; Witt-Eickschen & Kramm, 1998; Witt-Eickschen *et al.*, 1998, 2003). Most of these peridotite xenoliths are less radiogenic in Nd and more radiogenic in Sr isotope composition, indicating that such sources cannot represent the source of the basanites. In terms of Pb isotope composition, however, there is broad overlap between the lithospheric spinel peridotites from the East and West Eifel and the basanites from the Siebengebirge. Conditions of equilibration of the lithospheric peridotite xenoliths from beneath the Eifel have been estimated to be mostly <2·0 GPa and <1100°C, corresponding to a depth of ~60 km (Witt-Eickschen & Kramm, 1998; Witt-Eickschen *et al.*, 1998, 2003). Therefore, the source of the basanites and nephelinites must be somewhat deeper in the mantle; most probably close to the thermal boundary layer (TBL; Wilson *et al.*, 1995b). The Sr–Nd–Pb

isotope composition of the basanites, as well as their similarity to OIB and other primitive alkaline mafic magmas from Central Europe, further suggests that the source of these mafic alkaline lavas is located close to the TBL, although some workers (Goes *et al.*, 1999; Wedepohl & Baumann, 1999) have suggested a deep mantle or asthenospheric origin (Wilson & Downes, 1991, 2006) for some primitive alkaline lavas from Europe.

Oxygen isotope data ($\delta^{18}O$) obtained for selected minerals from the basanites and alkali basalts range from 5·8 to 6·4‰ for olivine and from 6·2 to 6·8‰ for clinopyroxene (Supplementary Data, Electronic Appendix Table 3). Because olivine and clinopyroxene are commonly unaltered or alteration-related features can be eliminated through acid leaching, these values can be used to estimate the oxygen isotope composition of the mantle source of the host basalts. These values show that the upper mantle beneath the Rhenish Shield has $\delta^{18}O$ values higher than mid-ocean ridge basalt (MORB; 5·7 ± 0·2‰; Harmon & Hoefs, 1995) but similar values to an alteration-corrected estimate for the Rhön lavas (5·5–6·7‰; Jung & Hoernes, 2000) and an average of continental intraplate basalts (6·1 ± 0·7; Harmon & Hoefs, 1995).

It has been suggested that the Cenozoic volcanism in Central Europe is related to two distinct mantle sources (Wilson & Downes, 1991, 2006; Wilson & Patterson, 2001). One common mantle source [the European Asthenospheric Reservoir (EAR) of Cebriá & Wilson (1995) or Low Velocity Component (LVC) of Hoernle *et al.* (1995)] has FOZO-like isotope characteristics and is inferred to be the source of the most primitive sodium-rich basalts whereas another, more enriched mantle source (EM I) contributed to the geochemistry of the more K_2O-rich basalts (Wörner *et al.*, 1986). The EAR component is probably transported from mantle regions deeper than the lithosphere–asthenosphere boundary in small-scale mantle plumelets (Granet *et al.*, 1995), one of which seems to exist beneath the Eifel (Ritter *et al.*, 2001; Keyser *et al.*, 2002). Considering the high $^{206}Pb/^{204}Pb$ ratios of the Siebengebirge lavas, it seems that these lavas are dominated by the EAR component, which is isotopically similar to an estimate of the TBL (Wilson *et al.*, 1995b). High $^{206}Pb/^{204}Pb$ ratios (>19·4) have been found only in some Quaternary West Eifel lavas (Wörner *et al.*, 1986) and in some mafic lavas from the Westerwald and the Hocheifel (Haase *et al.*, 2004; Jung *et al.*, 2006). Excluding the Quaternary West Eifel lavas, the high $^{206}Pb/^{204}Pb$ ratios of the Westerwald, Siebengebirge and Hocheifel lavas probably imply that these volcanic centres were fed from melts of the same mantle source during the Tertiary. The new Siebengebirge data presented here, with several mafic lavas having $^{206}Pb/^{204}Pb > 19{\cdot}4$, indicate that the EAR component is an important constituent of the upper mantle beneath the Rhenish Massif.

Evidence of regionally distinct upper mantle and lower crustal compositions

Previous isotope investigations on the volcanic rocks erupted in the Rhenish Massif have revealed substantial heterogeneities between the various volcanic fields. Haase *et al.* (2004) postulated that a distinct isotope boundary exists between the western (Eifel, Siebengebirge, Westerwald) and eastern volcanic fields (Vogelsberg, Rhön, Hessian Depression). For Nd and Sr isotopes there is remarkable overlap in isotope composition for most lavas from all fields (Jung & Masberg, 1998; Jung & Hoernes, 2000; Bogaard & Wörner, 2003; Haase et al., 2004; Jung *et al.*, 2005, 2006, 2011). The most distinctive feature is the variation in Pb isotope compositions and, in particular, the variation in $^{206}Pb/^{204}Pb$. Alkaline lavas from the Rhön and the Vogelsberg have $^{206}Pb/^{204}Pb$ ratios between 19·0 and 19·5 (Wedepohl & Baumann, 1999; Bogaard & Wörner, 2003; Jung *et al.*, 2005, 2011) whereas lavas from the Westerwald and Siebengebirge have $^{206}Pb/^{204}Pb$ ratios ranging from ~19·4 to ~19·8 (Haase *et al.*, 2004; this study). Only the Hocheifel data show complete overlap in $^{206}Pb/^{204}Pb$ ratios (~19·0 to ~20·0; Jung *et al.*, 2006). These features probably imply that two different mantle sources existed beneath the Rhenish Shield during the Eocene, Miocene and Oligocene.

There are also substantial differences in the ages of the volcanism between the different areas. Volcanism in the Tertiary Hocheifel occurred between 35 and 30 Ma (Fekiakova, 2004), followed by volcanic activity in the Westerwald between 28 and 21 Ma (Lippolt, 1982) and the Siebengebirge at about 28–23 Ma (Vieten *et al.*, 1988), in which all primitive lavas have high $^{206}Pb/^{204}Pb$ ratios >19·4. Volcanism in the eastern field (Vogelsberg, Rhön) occurred at 23–16 Ma in the Vogelsberg and at 26–11 Ma in the Rhön, producing primitive alkaline lavas with $^{206}Pb/^{204}Pb < 19{\cdot}5$. Irrespective of whether the single-plume model (Hoernle *et al.*, 1995) or the multiple-plumelet model is invoked (Wilson & Downes, 2006), the relationship between the ages and the isotope composition suggests some pulsing of the plume(s). In this case, the lavas from the Hocheifel (Jung *et al.*, 2006), Siebengebirge (this study) and the Westerwald (Haase *et al.*, 2004) have a greater contribution from a source with a higher $^{206}Pb/^{204}Pb$ ratio and the lavas from the Vogelsberg and the Rhön most probably represent partial melts from a source with a lower $^{206}Pb/^{204}Pb$ ratio. This model contradicts the view of Wedepohl & Baumann (1999), who suggested a contemporaneity of the volcanic phases that started at the margin of the inferred plume activity (Hocheifel in the west and Heldburg in the east) and proceeded toward the centre in the Siebengebirge, Westerwald and Rhön. Finally, volcanic activity occurred in the Vogelsberg and Hessian Depression. This model is also inconsistent with the Pb isotope composition

of the lavas, as the Hocheifel lavas belong to the high-$^{206}Pb/^{204}Pb$ group whereas the Heldburg lavas probably belong to the low-$^{206}Pb/^{204}Pb$ group ($^{206}Pb/^{204}Pb$ 19·15); although only one sample was analysed by Wedepohl & Baumann (1999). Similarly, the Westerwald and Siebengebirge lavas have high $^{206}Pb/^{204}Pb$ ratios but the Rhön lavas have low $^{206}Pb/^{204}Pb$ ratios. Only the Vogelsberg and Hessian Depression lavas have low $^{206}Pb/^{204}Pb$ ratios.

It seems that there are also substantial differences in the crustal composition beneath the various volcanic centres. For the Westerwald region, Haase *et al.* (2004) suggested that the lower crust contaminating the lavas has $^{87}Sr/^{86}Sr > 0{\cdot}706$ and $^{206}Pb/^{204}Pb > 19{\cdot}2$, whereas the crust contaminating the Vogelsberg lavas has $^{87}Sr/^{86}Sr < 0{\cdot}7045$ and $^{206}Pb/^{204}Pb < 18{\cdot}6$ as well as lower $^{143}Nd/^{144}Nd$ and $^{207}Pb/^{204}Pb$. If the isotope data from the contaminated lavas can be used to infer the nature of the contaminant, the isotope features seem to suggest that the lower crust beneath the Eifel, Siebengebirge and Westerwald is dominantly composed of rocks having high $^{87}Sr/^{86}Sr$, low $^{143}Nd/^{144}Nd$ and high $^{207}Pb/^{204}Pb$ at a given $^{206}Pb/^{204}Pb$ (Stosch & Lugmair, 1984; Rudnick & Goldstein, 1990); that is, representing most probably felsic granulites. On the other hand, the lower crust beneath the Vogelsberg, Rhön and the Hessian Depression contains a substantial amount of rocks with high $^{143}Nd/^{144}Nd$, low $^{87}Sr/^{86}Sr$ and moderate $^{207}Pb/^{204}Pb$ and $^{206}Pb/^{204}Pb$ ratios; that is, representing mafic granulites. This suggestion is compatible with new isotope data from the Rhön (Jung *et al.*, 2005) and the Vogelsberg (Jung *et al.*, 2011) where Os isotope systematics indicate that crustal contamination involves at least one mafic endmember. These suggestions are also compatible with the EC-AFC model calculations (Spera & Bohrson, 2001) of Bogaard & Wörner (2003), Haase *et al.* (2004) and Jung *et al.* (2006), who used the composition of a typical lower crustal granulite [sample S 35 from Stosch & Lugmair (1984)] to reproduce the isotope systematics of contaminated lavas from the Vogelsberg, Westerwald and Hocheifel areas. Haase *et al.* (2004) also observed slightly higher $^{207}Pb/^{204}Pb$ ratios in lavas from the Eifel group (Hocheifel, Siebengebirge, Westerwald) relative to the Vogelsberg group lavas (Vogelsberg, Hessian Depression), which they attributed to the higher $^{207}Pb/^{204}Pb$ ratios of the lower crustal contaminant beneath the Eifel. Indeed, lower crustal xenoliths have higher $^{207}Pb/^{204}Pb$ ratios at a given $^{206}Pb/^{204}Pb$ ratio relative to the host basalts (Rudnick & Goldstein, 1990). For the differentiated Siebengebirge lavas, $^{207}Pb/^{204}Pb$ ratios are higher relative to the mafic lavas, indicating the involvement of an ancient component having a high U/Pb ratio in the evolution of the differentiated rocks. This component is characterized by high $^{87}Sr/^{86}Sr$, low $^{143}Nd/^{144}Nd$, high $^{207}Pb/^{204}Pb$ and moderate $^{208}Pb/^{204}Pb$ and $^{206}Pb/^{204}Pb$ ratios.

CONCLUSIONS

Geochemical and isotopic studies of Tertiary Siebengebirge basanites, alkali basalts and more differentiated lavas provide the following constraints on the evolution of these rocks.

(1) Most of the investigated samples are relatively primitive basanites with high Mg# (mostly >0·60) and moderately high Cr and Ni contents. Some samples represent more differentiated magmas that have undergone polybaric fractionation of olivine + clinopyroxene + amphibole ± plagioclase + Fe–Ti oxides.

(2) Incompatible trace element abundances are remarkably similar for basanites and alkali basalts, and alkali basalts tend to have similar K/Nb, Rb/Nb, Zr/Nb, La/Nb and Ba/La but higher Ba/Nb ratios compared with basanites. Variations in REE abundances and correlations between REE ratios are compatible with partial melting of amphibole-bearing spinel peridotite. The presence of residual amphibole requires melting close to the asthenosphere–lithosphere boundary [close to the base of the TBL according to Wilson *et al.* (1995b)]. Using recent thermobarometry model calculations, the depth of melting for the most primitive lavas can be constrained at ~70–90 km at temperatures of ~1350°C. These estimates, however, are incompatible with the stability of amphibole in peridotite (Green *et al.*, 2010). The incompatible trace element enriched but isotopically depleted nature of the basalts requires a recently enriched mantle source.

(3) The Sr–Nd–Pb isotope compositions of the basanites and alkali basalts overlap and are broadly similar to those of other mafic lavas from the CEVP. The isotope characteristics imply the existence of a common mantle source for the Siebengebirge lavas that is broadly similar to an asthenospheric OIB-type source (EAR: Cebria & Wilson, 1995; LVC: Hoernle *et al.*, 1995). A comparison of Pb isotope variations seen in mafic rocks from the Siebengebirge, Hocheifel and Westerwald volcanic fields with mafic lavas of the Vogelsberg and Rhön volcanic fields may point to the existence of two different mantle sources beneath these lava fields.

(4) One alkaline basalt has a lower $^{206}Pb/^{204}Pb$ (18·98) and $^{207}Pb/^{204}Pb$ ratio (15·59) but similar $^{143}Nd/^{144}Nd$ and $^{87}Sr/^{86}Sr$ ratios compared with the basanites. The relatively unradiogenic Pb isotope composition is similar to some lavas from the Hessian Depression, Vogelsberg, Westerwald and Hocheifel representing the lower limit of $^{206}Pb/^{204}Pb$ and $^{207}Pb/^{204}Pb$ ratios found in CEVP lavas. The more differentiated samples have also assimilated material from the lower crust. Here, Pb isotope variations are characterized by high $^{207}Pb/^{204}Pb$ at constant $^{206}Pb/^{204}Pb$ ratios. There

must be substantial variations in the lower crustal compositions between the western lava fields (Hocheifel, Westerwald, Siebengebirge) and the eastern lava fields (Vogelsberg, Rhön, Hessian Depression) of the CEVP.

(5) It is generally accepted that volcanism in the CEVP is related to mantle metasomatism *sensu lato* (Wilson & Downes, 1991). It has recently been shown that mantle metasomatism related to carbonatite–peridotite interaction produces carbonated silicate partial melts with compositions that have many of the features of primitive alkaline volcanic rocks (Dasgupta *et al.*, 2006, 2007). Carbonated silicate melts are potentially parental to alkaline mafic magmas and may be produced at small degrees (1–5%) of partial melting from garnet peridotite with 0·1–0·25 wt % CO_2. These melts may form at *c.* 1350–1450°C at 3 GPa (Dasgupta *et al.*, 2007), conditions that could be encountered along the colder periphery of mantle plumes at about 90 km depth. Application of newly formulated thermobarometric expressions seems to confirm this view and similar P–T conditions were independently confirmed by Haase *et al.* (2004) and Jung *et al.* (2006) for the nearby Westerwald and Hocheifel lava fields. It is proposed here that melting below the Siebengebirge occurred at somewhat shallower depths, because of the observation that most lavas come from a spinel peridotite source. Carbonated silicate melts may infiltrate and metasomatize peridotite mantle leading to a TiO_2- and FeO-enriched carbonated peridotite with enriched trace element but depleted isotopic signatures (Dasgupta *et al.*, 2006, 2007). A scenario involving partial melts from carbonated peridotite may allow for the formation of alkalic volcanic rocks over a wider range of pressures and melt fractions than would otherwise be possible from unmetasomatized peridotite.

ACKNOWLEDGEMENTS

S.J. would like to thank E. Thun and J. Richarz (Hamburg) for XRF measurements and preparation of acid solutions. A. Klügel (Bremen) is thanked for providing ICP-MS trace element data. S.J. thanks H. Beier (Münster) for considerable help in the clean laboratory, for patience during the mass spectrometer measurements, and for her efforts to make the Sr–Nd–Pb measurements possible at short notice. Considerable thanks also go to Iris Bambach (Mainz) for her patience during managing of the line drawings. We appreciate the detailed comments by H. G. Stosch, G. Fitton, M. Wilson and an anonymous reviewer, which helped to improve the paper.

FUNDING

KV and SH appreciate funding through various grants from the Deutsche Forschunggemeinschaft over the years.

SUPPLEMENTARY DATA

Supplementary data for this paper are available at *Journal of Petrology* online.

REFERENCES

Alibert, C., Leterrier, J., Panasiuk, M. & Zimmermann, J. L. (1987). Trace and isotope geochemistry of the alkaline Tertiary volcanism in southwest Poland. *Lithos* **20**, 311–321.

Allègre, C. J., Dupré, B., Lambert, B. & Richard, P. (1981). The subcontinental versus suboceanic debate, I. Lead–neodymium–strontium isotopes in primary alkali basalts from a shield area: the Ahaggar volcanic suite. *Earth and Planetary Science Letters* **52**, 85–92.

Babuska, V. & Plomerová, J. (1988). Subcrustal continental lithosphere: a model of its thickness and anisotropic structure. *Physics of the Earth and Planet Interiors* **51**, 130–132.

Babuska, V. & Plomerová, J. (1992). The lithosphere in central Europe—seismological and petrological aspects. *Tectonophysics* **207**, 141–163.

Babuska, V. & Plomerová, J. (2006). European mantle lithosphere assembled from rigid microplates with inherited seismic anisotropy. *Physics of the Earth and Planetary Interiors* **158**, 264–280.

Baker, J. A., Menzies, M. A., Thirlwall, M. F. & MacPherson, C. G. (1997). Petrogenesis of Quaternary intraplate volcanism, Sana'a, Yemen: Implications for plume–lithosphere interaction and polybaric melt hybridization. *Journal of Petrology* **38**, 1359–1390.

Blusztajn, J. & Hart, S. R. (1989). Sr, Nd, and Pb isotopic character of Tertiary basalts from southwest Poland. *Geochimica et Cosmochimica Acta* **53**, 2689–2696.

Blusztajn, J. & Hegner, E. (2002). Osmium isotopic systematics of melilitites from the Tertiary Central European Volcanic province in SW Germany. *Chemical Geology* **189**, 91–103.

Bogaard, P. F. J. & Wörner, G. (2003). Petrogenesis of basanitic to tholeiitic volcanic rocks from the Miocene Vogelsberg, Central Germany. *Journal of Petrology* **44**, 569–602.

Boynton, W. V. (1984). Geochemistry of the rare earth elements: meteorite studies. In: Henderson, P. (ed.) *Rare Earth Element Geochemistry*. Amsterdam: Elsevier, pp. 63–114.

Brey, G. & Green, D. H. (1977). Systematic study of liquidus phase relations in olivine melilitite + H_2O + CO_2 at high pressures and petrogenesis of an olivine melilitite magma. *Contributions to Mineralogy and Petrology* **61**, 141–162.

Cameron, A. E., Smith, D. H. & Walker, R. L. (1969). Mass spectrometry of nanogram-size samples of lead. *Analytical Chemistry* **41**, 525–526.

Cebria, J. M. & Wilson, M. (1995). Cenozoic mafic magmatism in Western/Central Europe: a common European asthenospheric reservoir? *Terra Nova Abstracts Supplement* **7**, 162.

Class, C. & Goldstein, S. L. (1997). Plume–lithosphere interaction in the ocean basins: contraints from source mineralogy. *Earth and Planetary Science Letters* **150**, 245–260.

Clayton, R. N. & Mayeda, T. D. (1963). The use of bromine pentafluoride in the extraction of oxygen from oxides and silicates for isotope analysis. *Geochimica et Cosmochimica Acta* **27**, 43–52.

Dasgupta, R. & Hirschmann, M. M. (2006). Melting in the Earth's deep upper mantle caused by carbon dioxide. *Nature* **440**, 659–662.

Dasgupta, R., Hirschmann, M. M. & Smith, N. D. (2007). Partial melting experiments of peridotite + CO_2 at 3 GPa and genesis of alkalic ocean island basalts. *Journal of Petrology* **48**, 2093–2124.

Dasgupta, R., Hirschmann, M. M. & Stalker, K. (2006). Immiscible transition from carbonate-rich to silicate-rich melts in the 3 GPa melting interval of eclogite + CO_2 and genesis of silica-undersaturated ocean island lavas. *Journal of Petrology* **47**, 647–671.

Downes, H. (1984). Sr and Nd isotope geochemistry of coexisting alkaline magma series, Cantal, Massif Central, France. *Earth and Planetary Science Letters* **69**, 321–334.

Downes, H., Seghedi, I., Szakacs, A., Dobosi, G., James, D. E., Vasselli, O., Rigby, I. J., Ingram, G. A., Rex, D. & Pecskay, Z. (1995). Petrology and geochemistry of late Tertiary/Quaternary mafic alkaline volcanism in Romania. *Lithos* **35**, 65–81.

Duda, A. & Schmincke, H. U. (1985). Polybaric differentiation of alkali basaltic magma: evidence from green-core clinopyroxenes (Eifel, Germany). *Contributions to Mineralogy and Petrology* **91**, 340–351.

Embey-Isztin, E., Downes, H., James, D. E., Upton, B. G. J., Dobosi, G., Ingram, G. A., Harmon, R. S. & Scharbert, H. G. (1993). The petrogenesis of Pliocene alkaline volcanic rocks from the Pannonian Basin, Eastern Central Europe. *Journal of Petrology* **34**, 317–343.

Engelhardt, H.-J. (1990). TUC-Referenzproben in Geochemie und Umweltanalytik. *Mitteilungsblatt TU Clausthal* **70**, 26–28.

Falloon, T. J. & Green, D. H. (1990). Solidus of carbonated fertile peridotite under fluid-saturated conditions. *Geology* **18**, 195–199.

Fekiacova, Z. (2004). Geochronology, geochemistry and isotopic composition of the volcanic rocks from oceanic (Hawaii) and continental (Eifel) intra-plate environments, PhD dissertation, University of Mainz, 109 pp.

Ferrara, G., Laurenzi, M. A., Taylor, H. P., Toranini, S. & Turi, P. (1985). Oxygen and strontium isotope studies of K-rich volcanic rocks from the Alban Hill, Italy. *Earth and Planetary Science Letters* **75**, 13–28.

Fitton, J. G. & Dunlop, H. M. (1985). The Cameroon Line, West Africa, and its bearing on the origin of oceanic and continental alkali basalts. *Earth and Planetary Science Letters* **72**, 23–38.

Foley, S. (1991). High-pressure stability of the fluor- and hydroxy-endmembers of pargasite and K-richterite. *Geochimica et Cosmochimica Acta* **55**, 2689–2694.

Frey, F. A., Green, D. H. & Roy, S. D. (1978). Integrated models of basalt petrogenesis: A study of quartz tholeiites to olivine melilitites from South Eastern Australia utilizing geochemical and experimental petrological data. *Journal of Petrology* **19**, 463–513.

Gallagher, K. & Hawkesworth, C. J. (1992). Dehydration melting and the generation of continental flood basalts. *Nature* **358**, 57–59.

Goes, S., Spakman, H. & Bijwaard, H. (1999). A lower mantle source for Central European volcanism. *Science* **286**, 1928–1931.

Govindaraju, K. (ed) (1994). Compilation of working values and sample description for 383 geostandards. *Geostandards Newsletter* **17**, 158 p.

Granet, M., Wilson, M. & Achauer, U. (1995). Imaging a mantle plume beneath the French Massif Central. *Earth and Planetary Science Letters* **136**, 281–296.

Green, D. H., Hibberson, W. O., Kovacs, I. & Rosenthal, A. (2010). Water and its influence on the lithosphere/asthenosphere boundary. *Nature* **467**, 448–451.

Haase, K. M. & Renno, A. D. (2008). Variation of magma generation and mantle sources during continental rifting observed in Cenozoic lavas from the Eger Rift, Central Europe. *Chemical Geology* **257**, 192–202.

Haase, K. M., Goldschmidt, B. & Garbe-Schönberg, D. (2004). Petrogenesis of Tertiary continental intra-plate lavas from the Westerwald region, Germany. *Journal of Petrology* **45**, 883–905.

Harangi, S. (1994). Geochemistry and petrogenesis of the early Cretaceous continental rift-type volcanic rocks of the Mecsek Mountains, South Hungary. *Lithos* **33**, 303–321.

Harmon, R. S. & Hoefs, J. (1995). Oxygen isotope heterogeneity of the mantle deduced from global ^{18}O systematics of basalts from different geotectonic settings. *Contributions to Mineralogy and Petrology* **120**, 95–114.

Harry, D. L. & Leeman, W. P. (1995). Partial melting of melt metasomatized subcontinental mantle and the magma source potential of the lower lithosphere. *Journal of Geophysical Research* **100**, 10255–10269.

Hart, S. R. (1984). A large-scale isotope anomaly in the southern hemisphere mantle. *Nature* **309**, 753–757.

Hart, S. R. (1988). Heterogeneous mantle domains: signatures, genesis, and mixing chronologies. *Earth and Planetary Science Letters* **90**, 273–296.

Hart, S. R. & Davis, K. E. (1978). Nickel partitioning between olivine and silicate melt. *Earth and Planetary Science Letters* **40**, 203–219.

Hart, S. R. & Dunn, T. (1993). Experimental clinopyroxene/melt partitioning of 24 trace elements. *Contributions to Mioneralogy and Petrology* **113**, 1–8.

Hartmann, G. & Wedepohl, K. H. (1990). Metasomatically altered peridotite xenoliths from the Hessian Depression (Northwest Germany). *Geochimica et Cosmochimica Acta* **54**, 71–86.

Hegner, E., Walter, H. J. & Satir, M. (1995). Pb–Sr–Nd isotopic compositions and trace element geochemistry of megacrysts and melilitites from the Tertiary Urach volcanic field: source composition of small volume melts under SW Germany. *Contributions to Mineralogy and Petrology* **122**, 322–335.

Heinrichs, H. & Herrmann, A. G. (1990). *Praktikum der Analytischen Geochemie*. Springer: Berlin.

Hirose, K. (1997). Partial melt compositions of carbonated peridotite at 3 GPa and role of CO_2 in alkali-basalt magma generation. *Geophysical Research Letters* **24**, 2837–2840.

Hirschmann, M. M. (2000). The mantle solidus: experimental constraints and the effect of peridotite composition. *Geochemistry, Geophysics, Geosystems* **1**, paper number 2000GC000070.

Hirschmann, M. M., Kogiso, T., Baker, M. B. & Stolper, E. M. (2003). Alkalic magmas generated by partial melting of garnet pyroxenite. *Geology* **31**, 481–484.

Hoernle, K., Zhang, Y.-S. & Graham, D. (1995). Seismic and geochemical evidence for large-scale mantle upwelling beneath the eastern Atlantic and western and central Europe. *Nature* **374**, 34–39.

Hofmann, A. W. (1997). Mantle geochemistry: The message from oceanic volcanism. *Nature* **385**, 219–229.

Hofmann, A. W., Jochum, K. P., Seufert, M. & White, W. M. (1986). Nb and Pb in oceanic basalts: new constraints on mantle evolution. *Earth and Planetary Science Letters* **79**, 33–45.

Johnson, K. T. M. (1998). Experimental determination of partition coefficients for rare earth and high-field-strength elements between clinopyroxene, garnet, and basaltic melt at high pressures. *Contributions to Mineralogy and Petrology* **133**, 60–68.

Jung, S. & Hoernes, S. (2000). The major- and trace element and isotope (Sr, Nd, O) geochemistry of Cenozoic alkaline rift-type volcanic rocks from the Rhön area (central Germany): Petrology, mantle source characteristics and implications for asthenosphere–lithosphere interactions. *Journal of Volcanology and Geothermal Research* **99**, 27–53.

Jung, S. & Masberg, P. (1998). Major- and trace element systematics and isotope geochemistry of Cenozoic mafic volcanic rocks from

the Vogelsberg (Central Germany)—constraints on the origin of continental alkaline and tholeiitic basalts and their mantle sources. *Journal of Volcanology and Geothermal Research* **86**, 151–177.

Jung, S., Pfänder, J. A., Brügmann, G. & Stracke, A. (2005). Sources of primitive alkaline volcanic rocks from the Central European Volcanic Province (Rhön, Germany) inferred from Hf, Os and Pb isotopes. *Contributions to Mineralogy and Petrology* **150**, 546–559.

Jung, C., Jung, S., Hoffer, E. & Berndt, J. (2006). Petrogenesis of Tertiary mafic alkaline magmas in the Hocheifel, Germany. *Journal of Petrology* **47**, 1637–1671.

Jung, S., Pfänder, J. A., Brauns, M. & Maas, R. (2011). Crustal contamination and mantle source characteristics in continental intra-plate volcanic rocks: Pb, Hf and Os isotopes from central European volcanic province basalts. *Geochimica et Cosmochimica Acta* **75**, 2664–2683.

Kelemen, P. B., Shimizu, N. & Dunn, T. (1993). Relative depletion of niobium in some arc magmas and the continental crust: partitioning of K, Nb, La and Ce during melt/rock reaction in the upper mantle. *Earth and Planetary Science Letters* **120**, 111–134.

Kemp, A. I. S. & Hawkesworth, C. J. (2004). Granitic perspectives on the generation and secular evolution of the continental crust. In: Holland, H. D. & Turekian, K. K. (eds) *Treatise on Geochemistry, Vol. 3*. Amsterdam: Elsevier, pp. 349–410.

Keshav, S., Gudfinnsson, G. H., Sen, G. & Fei, Y. (2004). High-pressure melting experiments on garnet clinopyroxenite and the alkalic to tholeiitic transition in ocean-island basalts. *Earth and Planetary Science Letters* **223**, 365–379.

Keyser, M., Ritter, J. R. R. & Jordan, M. (2002). 3D shear-wave velocity structure of the Eifel plume, Germany. *Earth and Planetary Science Letters* **203**, 59–82.

Kogiso, T., Hirschmann, M. M. & Frost, D. J. (2003). High-pressure partial melting of garnet pyroxenite: possible mafic lithologies in the source of ocean island basalts. *Earth and Planetary Science Letters* **216**, 603–617.

Kushiro, I. (1996). Partial melting of a fertile mantle peridotite at high pressures: an experimental study using aggregates of diamond. In: Basu, A. & Hart, S. R. (eds) *Earth Processes: Reading the Isotopic Code. Geophysical Monograph, American Geophysical Union* **95**, 109–122.

LaTourrette, T., Hervig, R. L. & Holloway, J. R. (1995). Trace element partitioning between amphibole, phlogopite, and basanite melt. *Earth and Planetary Science Letters* **135**, 13–30.

Le Bas, M. J., Le Maitre, R. W., Streckeisen, A. & Zanettin, B. (1986). A chemical classification of volcanic rocks based on the total alkali–silica diagram. *Journal of Petrology* **27**, 745–750.

Lechler, P. J. & Desilets, M. O. (1987). A review of the use of loss on ignition as a measurement of total volatiles in whole-rock analysis. *Chemical Geology* **63**, 341–344.

Lee, C.-T. A., Luffi, P., Plank, T., Dalton, H. & Leeman, W. P. (2009). Constraints on the depths and temperatures of basaltic magma generation on Earth and other terrestrial planets using new thermobarometers for mafic magmas. *Earth and Planetary Science Letters* **279**, 20–33.

Le Maitre, R. W. (ed.), Streckeisen, A., Zanettin, B., Le Bas, M. J., Bonin, B., Bateman, P., Bellieni, G., Dudek, A., Efremova, S., Keller, J., Lameyre, J., Sabine, P. A., Schmid, R., Sorensen, H. & Woolley, A. R. (2002). *Igneous Rocks: A Classification and Glossary of Terms, Recommendations of the International Union of Geological Sciences, Subcommission of the Systematics of Igneous Rocks*. Cambridge: Cambridge University Press.

Lenardic, A., Moresi, L.-N., Jellinek, A. M. & Manga, M. (2005). Continental insulation, mantle cooling, and the surface area of oceans and continents. *Earth and Planetary Science Letters* **234**, 317–333.

Lippolt, H. J. (1982). K/Ar age determinations and the correlation of Tertiary volcanic activity in Central Europe. *Geologisches Jahrbuch Hannover* **D52**, 113–135.

Loock, G., Stosch, H.-G. & Seck, H. A. (1990). Granulite facies lower crustal xenoliths from the Eifel, West Germany: petrological and geochemical aspects. *Contributions to Mineralogy and Petrology* **195**, 25–41.

Lustrino, M. & Wilson, M. (2007). The circum-Mediterranean anorogenic Cenozoic igneous province. *Earth-Science Reviews* **81**, 1–65.

Mattinson, J. M. (1986). Geochronology of high-pressure–low temperature Franciscan metabasites. A new approach using the U–Pb system. *Geological Society of America, Memoirs* **164**, 95–105.

McKenzie, D. & Bickle, M. J. (1988). The volume and composition of melt generated by extension of lithosphere. *Journal of Petrology* **29**, 625–679.

McKenzie, D. & O'Nions, R. K. (1983). Mantle reservoirs and ocean island basalts. *Nature* **301**, 229–331.

McKenzie, D. & O'Nions, R. K. (1991). Partial melt distributions from inversion of rare earth element concentrations. *Journal of Petrology* **32**, 1021–1091.

Mengel, K. & Green, D. H. (1986). Stability of amphibole and phlogopite in metasomatized peridotite under water-saturated and water-undersaturated conditions. In: Ross, J., Jaques, A. L., Ferguson, J., Green, D. H., O'Reilly, S. Y., Danchin, R. V. & Janse, A. J. A. (eds) *Kimberlites and Related Rocks, 1.* Oxford: Blackwell Scientific, pp. 571–581.

Mengel, K., Sachs, P. M., Stosch, H. G., Wörner, G. & Loock, G. (1991). Crustal xenoliths from Cenozoic volcanic fields of West Germany: implications for structure and composition of the crust. *Tectonophysics* **195**, 271–289.

Mysen, B. O. & Kushiro, I. (1977). Compositional variations of coexisting phases with degree of melting of peridotite in the upper mantle. *American Mineralogist* **62**, 843–865.

Niu, Y. & O'Hara, M. J. (2003). Origin of ocean island basalts: A new perspective from petrology, geochemistry, and mineral physics considerations. *Journal of Geophysical Research* **108(B4)**, 2209–2228.

Pilet, S., Baker, M. B. & Stolper, E. M. (2008). Metasomatized lithosphere and the origin of alkaline lavas. *Science* **320**, 916–919.

Prodehl, C., Müller, S., Glahn, A., Gutsher, M. & Haak, V. (1992). Lithosphere cross-section of the European rift system. *Tectonophysics* **208**, 113–138.

Rapp, R. P., Watson, E. B. & Miller, C. F. (1991). Partial melting of amphibolite/eclogite and the origin of Archean trondhjemites and tonalites. *Precambrian Research* **51**, 1–25.

Reiners, P. W., Nelson, B. K. & Ghiorso, M. S. (1995). Assimilation of felsic crust by basaltic magma: Thermal limits and extents of crustal contamination of mantle-derived magmas. *Geology* **23**, 563–566.

Ritter, J. R. R., Jordan, M., Christensen, U. R. & Achauer, U. (2001). A mantle plume below the Eifel volcanic fields, Germany. *Earth and Planetary Science Letters* **186**, 7–14.

Robinson, J. A. C. & Wood, B. J. (1998). The depth of the spinel to garnet transition at the peridotite solidus. *Earth and Planetary Science Letters* **164**, 277–284.

Romer, R. L. & Hahne, K. (2010). Life of the Rheic Ocean: Scrolling through the shale record. *Gondwana Research* **17**, 236–253.

Rosenbaum, J. M. (1993). Mantle phlogopite: a significant lead repository. *Chemical Geology* **106**, 457–483.

Rudnick, R. L. & Gao, S. (2004). Composition of the continental crust. In: Holland, H. D. & Turekian, K. K. (eds) *Treatise on Geochemistry, Vol. 3*. Amsterdam: Elsevier, pp. 1–64.

Rudnick, R. & Goldstein, S. L. (1990). The Pb isotopic evolution of lower crustal xenoliths and the evolution of lower crustal Pb. *Earth and Planetary Science Letters* **98**, 192–207.

Sachs, P. M. & Hansteen, T. H. (2000). Pleistocene underplating and metasomatism of the lower continental crust: a xenolith study. *Journal of Petrology* **41**, 331–356.

Shaw, D. M. (1970). Trace element fractionation during anatexis. *Geochimica et Cosmochimica Acta* **34**, 237–243.

Sobolev, A. V., Hofmann, A. W., Sobolev, S. V. & Nikogosian, I. K. (2005). An olivine-free mantle source of Hawaiian shield basalts. *Nature* **434**, 590–597.

Sobolev, A. V., Hofmann, A. W., Kuzmin, D. V. *et al.* (2007). The amount of recycled crust in sources of mantle-derived melts. *Science* **316**, 412–417.

Spandler, C., Yaxley, G., Green, D. H. & Rosenthal, A. (2008). Phase relations and melting of anhydrous K-bearing eclogite from 1200 to 1600°C and 3 to 5 GPa. *Journal of Petrology* **49**, 771–795.

Spera, F. J. & Bohrson, W. A. (2001). Energy-constrained open-system magmatic processes; I, General model and energy-constrained assimilation and fractional crystallization (EC-AFC) formulation. *Journal of Petrology* **42(5)**, 999–1018.

Stosch, H.-G. & Lugmair, G. W. (1984). Evolution of the lower continental crust: granulite facies xenoliths from the Eifel, West Germany. *Nature* **311**, 368–370.

Stosch, H.-G. & Lugmair, G. W. (1986). Trace element and Sr and Nd isotope geochemistry of peridotite xenoliths from the Eifel (West Germany) and their bearing on the evolution of the subcontinental lithosphere. *Earth and Planetary Science Letters* **80**, 281–298.

Stosch, H.-G. & Seck, H. A. (1980). Geochemistry and mineralogy of two spinel peridotite suites from Dreiser Weiher, West Germany. *Geochimica et Cosmochimica Acta* **44**, 457–470.

Stosch, H.-G., Lugmair, G. W. & Seck, H. A. (1986). Geochemistry of granulite-facies lower crustal xenoliths: implications for the geological history of the lower continental crust below the Eifel, West Germany. In: Dawson, J. B., Carswell, D. A., Hall, J. & Wedepohl, K. H. (eds) *The Nature of the Lower Continental Crust. Geological Society, London, Special Publications* **24**, 309–317.

Stosch, H.-G., Schmucker, A. & Reys, C. (1992). The nature and geological history of the deep crust under the Eifel, Germany. *Terra Nova* **4**, 53–62.

Sun, S.-S. & McDonough, W. F. (1989). Chemical and isotopic systematics of oceanic basalts: implications for mantle composition and processes. In: Saunders, A. D. & Norry, M. J. (eds) *Magmatism in the Ocean Basins. Geological Society, London, Special Publications* **42**, 313–345.

Thibault, Y., Edgar, A. D. & Lloyd, F. E. (1992). Experimental investigation of melts from a carbonated phlogopite lherzolite: implications for metasomatism in the continental lithosphere. *American Mineralogist* **77**, 784–794.

Thirlwall, M. F., Upton, B. G. J. & Jenkins, C. (1994). Interaction between continental lithosphere and the Iceland plume—Sr–Nd–Pb isotope chemistry of Tertiary basalts, NE Greenland. *Journal of Petrology* **35**, 839–897.

Thompson, R. N. & Morrison, M. A. (1988). Asthenospheric and lower-lithospheric mantle contributions to continental extensional magmatism: an example from the British Tertiary Province. *Chemical Geology* **68**, 1–15.

Todt, W. & Lippolt, H. J. (1980). K–Ar age determinations on Tertiary volcanic rocks: V: Siebengebirge, Siebengebirgsgraben. *Journal of Geophysical Research* **48**, 18–27.

van der Hilst, R. D., Widiyantoro, S. & Engdahl, E. R. (1997). Evidence for deep mantle circulation from global tomography. *Nature* **386**, 578–584.

Vieten, K., Hamm, H. M. & Grimmeisen, W. (1988). Tertiärer Vulkanismus im Siebengebirge. *Fortschritte der Mineralogie* **66(2)**, 1–39.

Vogel, W. & Kuipers, G. (1987). A pre-calibrated program for geological applications. *Phillips New Developments X-Ray Spectrometry* **11**, 2–8.

Wedepohl, K. H. & Baumann, A. (1999). Central European Cenozoic plume volcanism with OIB characteristics and indications of lower mantle source. *Contributions to Mineralogy and Petrology* **136**, 225–239.

Wedepohl, K. H., Gohn, E. & Hartmann, G. (1994). Cenozoic alkali basaltic magmas of western Germany and their products of differentiation. *Contributions to Mineralogy and Petrology* **115**, 253–278.

White, W. M. & Hofmann, A. W. (1982). Sr and Nd isotope geochemistry of oceanic basalts and mantle evolution. *Nature* **296**, 821–825.

Wilson, M. & Downes, H. (1991). Tertiary–Quaternary extension-related alkaline magmatism in Western and Central Europe. *Journal of Petrology* **32**, 811–849.

Wilson, M. & Downes, H. (2006). Tertiary–Quaternary intra-plate magmatism in Europe and its relationship to mantle dynamics. In: Stephenson, R. A. & Gee, D. (eds) *European Lithosphere Dynamics. Geological Society, London, Memoirs* **32**, 147–166.

Wilson, M. & Patterson, R. (2001). Intra-plate magmatism related to hot fingers in the upper mantle: Evidence from the Tertiary–Quaternary volcanic province of western and central Europe. In: Ernst, R. & Buchan, K. (eds) *Mantle Plumes: their Identification through Time. Geological Society of America, Special Papers* **352**, 37–58.

Wilson, M., Downes, H. & Cebria, J.-M. (1995*a*). Contrasting fractionation trends in coexisting continental alkaline magma series; Cantal, Massif Central, France. *Journal of Petrology* **36**, 1729–1753.

Wilson, M., Rosenbaum, J. M. & Dunworth, E. A. (1995*b*). Melilitites: partial melts of the thermal boundary layer? *Contributions to Mineralogy and Petrology* **119**, 181–196.

Witt-Eickschen, G. & Kramm, U. (1998). Evidence for the multiple stage evolution of the subcontinental lithospheric mantle beneath the Eifel (Germany) from pyroxenite and composite pyroxenite/peridotite xenoliths. *Contributions to Mineralogy and Petrology* **131**, 258–272.

Witt-Eickschen, G., Kaminsky, W., Kramm, U. & Harte, B. (1998). The nature of young vein metasomatism in the lithosphere of the West Eifel (Germany): Geochemical and isotopic constraints from composite mantle xenoliths from the Meerfelder Maar. *Journal of Petrology* **39**, 155–185.

Witt-Eickschen, G., Seck, H. A., Mezger, K., Eggins, S. M. & Altherr, R. (2003). Lithospheric mantle evolution beneath the Eifel (Germany): Constraints from Sr–Nd–Pb isotopes and trace element abundances in spinel peridotite and pyroxenite xenoliths. *Journal of Petrology* **44**, 1077–1095.

Wörner, G., Zindler, A., Staudigel, H. & Schmincke, H. U. (1986). Sr, Nd, and Pb isotope geochemistry of Tertiary and Quaternary alkaline volcanics from West Germany. *Earth and Planetary Science Letters* **79**, 107–119.

Yaxley, G. M. & Green, D. H. (1998). Reactions between eclogite and peridotite: Mantle refertilization by subducted oceanic crust. *Schweizerische Mineralogische und Petrographische Mitteilungen* **78**, 243–255.

Ziegler, P. A. (1992). European Cenozoic rift system. *Tectonophysics* **208**, 91–111.